



Call: HORIZON-CL5-2021-D5-01

**Hyperconnected simulation ecosystem supporting probabilistic design
and predictive manufacturing of next generation aircraft structures**

CAELESTIS

Deliverable D4.2

RTM process Interoperable Digital Twin with process defect predictions

Work Package 4

Digital manufacturing and defects prediction

Document type : Report
Version : 1.0
Date of issue : 30/04/2024
Dissemination level : PUBLIC
Lead beneficiary : ITA

Funded by the European Union. Views and opinions expressed are however those of the author(s) only and do not necessarily reflect those of the European Union or [EUROPEAN CLIMATE, INFRASTRUCTURE AND ENVIRONMENT EXECUTIVE AGENCY (CINEA)]. Neither the European Union nor the granting authority can be held responsible for them.



Funded by the
European Union

The information contained in this report is subject to change without notice and should not be construed as a commitment by any members of the CAELESTIS Consortium. The information is provided without any warranty of any kind.

This document may not be copied, reproduced, or modified in whole or in part for any purpose without written permission from the CAELESTIS Consortium. In addition to such written permission to copy, acknowledgement of the authors of the document and all applicable portions of the copyright notice must be clearly referenced.

© COPYRIGHT 2020 The CAELESTIS Consortium.

All rights reserved.

Executive Summary

Abstract	The CAELESTIS project aims to establish an advanced Interoperable Simulation Ecosystem (ISE) that integrates product design, distributed engineering teams, and manufacturing experts to accelerate the development of next-generation aircraft. Central to CAELESTIS is the deployment of high-fidelity digital twins, facilitating accurate predictions throughout the product development cycle, including processes like automated fiber placement (AFP), laser powder bed fusion (L-PBF), and resin transfer molding (RTM). This deliverable focuses on the RTM and L-PBF Digital Twins within CAELESTIS, detailing the modeling strategies for manufacturing simulations, particularly emphasizing the fan outlet guide vane (FOGV) use case. The document elaborates on the meso-scale strategy developed for predicting void generation during RTM, incorporating bi-phasic computational fluid dynamics (CFD) simulations and PBF analysis of metallic inserts. Additionally, it outlines RTM process models from input data to distortion analysis, showcasing preliminary results.
Keywords	RTM process simulation, L-PBF process simulation, digital twin, multiscale simulation

Revision history

Version	Author(s)	Changes	Date
0.1	Francisco Serrano (ITA)	Table of Contents	18/03/2024
0.2	Tanguy Moro, Yvan Denis, Clément Freyssinnet (JV)	Contribution to sections 2 and 5.	02/04/2024
0.3	Mustafa Megahed Philippe Gellenne (ESI)	Contribution to sections 4 and 6	26/03/2024
0.4	Francisco Serrano (ITA) and Carmen Alfaro (ITA)	Contribution to sections 2 and 6. Sections 1 and 3.	08/04/2024
0.5	Francisco Serrano (ITA)	Format edits before internal review	12/04/2024
0.6	Verónica Mantecón (AIMEN)	Minor changes format	25/04/2023
0.7	Gerard Guillamet (BSC)	Reviewed	25/04/2024
0.8	Estelle Castanet (GKN)	Reviewed	26/04/2024
1.0	Francisco Serrano (ITA)	Address internal review comments	29/04/2024

TABLE OF CONTENTS

1	INTRODUCTION.....	7
2	RTM DIGITAL TWIN IN THE GLOBAL WORKFLOW	8
3	MULTISCALE VOIDS MODEL.....	13
3.1	Meshing.....	16
3.2	Case configuration.....	19
3.3	Workflow and HPC	30
3.4	First simulations	33
4	L-PBF SIMULATION.....	35
4.1	Material	36
4.2	Inner fitting distortion analysis	37
4.3	Outer fitting distortion analysis	39
5	RTM MODELLING & SIMULATION: RTM DIGITAL TWIN	40
5.1	Resin Transfer Molding (RTM) process for composite parts	40
5.2	RTM process modelling and simulation with PAM-RTM/DISTORTION®.....	41
5.3	Proofs Of Concepts 1, 2 and OGV. Strategy for Processes Digital Twins and numerical workflow.....	47
5.4	Proof Of Concept 1: RTM modelling and simulation	48
5.5	GKN’s OGV: RTM modelling and simulation	55
6	CONCLUSION AND FUTURE WORK (ITA, JVN, ESI)	65

LIST OF FIGURES

Figure 1: Numerical workflow for processes digital twins.	9
Figure 2: Numerical and physical data exchanged between ADDPath®, permeability ROM and PAM-RTM®.	11
Figure 3: RVE examples: a) traditional woven fabric, and b) AFP process fabric.	15
Figure 4: Model prediction and experimental measurement of multi-scale voids formation in woven fabric RTM process ²	15
Figure 5: Mesh of hexahedral elements (full domain and detail).	16
Figure 6: Mesh of tetrahedral elements (full domain and detail).	16
Figure 7: Mesh of voxels elements (full domain and detail).	16
Figure 8: Mesh of voxels elements with three layers of fibers. Orientation 0 degrees.	17
Figure 9: Mesh of voxels elements with increasing number of elements in Z (5, 10, and 15).	17
Figure 10: Comparison of velocity profiles in X and Y for meshes with increasing number of elements in Z direction.	18
Figure 11: Representation of the hybridPorousInterFoam approach for the simulation of multiphasic flow in hybrid porous media ⁴	21
Figure 12: CFD simulation of voids: simulation strategy imposing pressure drop in the monophasic simulation (ΔP) and velocity at the inlet (U_{inlet}).	26
Figure 13: CFD simulation of voids: boundary conditions.	27
Figure 14: CFD simulation of voids: porous media definition (solid indicator, porosity and permeability)	28
Figure 15: CFD simulation of voids: single-phase velocity and pressure fields.	28
Figure 16: CFD simulation of voids: initialization of biphasic simulation.	29
Figure 17: Workflow to generate the voids model.	31
Figure 18: RVE with small tows to analyze the simulations, a) shows the gaps between tows (blue), and b) shows the complete model.	33
Figure 19: Preliminary results showing gaps (blue) and tows (red) together with the flow front of the resin. a, b, c, and d show four different increasing times. (View 1).	34
Figure 20: Preliminary results showing gaps (blue) and tows (red) together with the flow front of the resin. a, b, c, and d show four different increasing times. (View 2).	35
Figure 21: Preliminary design of inner (left) and outer (right) fittings.	35
Figure 22: Build orientation of inner fitting: The Z axis shows the build direction.	38
Figure 23: Inner fitting computational grid for distortion analysis and support structure generated.	38
Figure 24: Distortion states after release of base plate clamps and after part removal via EDM for both a course grid calculation and a fine grid.	39
Figure 25: Distortion computational grid and support structure for inner fitting.	40
Figure 26: Inner distortion distribution.	40
Figure 27: Draping the stacking from UD tape with Automated Fiber Placement (AFP) process & Resin Transfer Molding (RTM) process for composite parts.	41
Figure 28: Permeabilities characterization and values function of fiber volume fraction (REF. 5.1). ..	45
Figure 29: Flat panel setup for the in plane permeabilities characterization (REF. 5.1).	45
Figure 30: Draping the stacking from UD tape with AFP (Automated Fiber Placement) process & defects on plies.	46
Figure 31: Dimensions and specifications of the composite plate POC1 and of the mold.	49

Figure 32: RTM mold for the manufacturing of the composite plate POC1.	49
Figure 33: FEM mesh with tetrahedron 3D elements of the POC1 & injection point location.....	50
Figure 34: Stacking of the plies of the preform of the POC1.	50
Figure 35: Temperature ramp for the curing phase of the POC 1.	51
Figure 36: RTM process simulation of the composite plate POC 1 manufacturing.	51
Figure 37: RTM process simulation and main results of the composite plate POC 1 manufacturing...	54
Figure 38: OGV first design and dimensions (REF. 5.2).	55
Figure 39: OGV first design and dimensions for composite vane.	56
Figure 40: Laminate ply table.	57
Figure 41: FEM mesh with tetrahedron 3D elements of the vane, injection strategy and "pseudo mold".....	58
Figure 42: Stacking of the plies of the preform of the vane.	58
Figure 43: Automatic layup of the stacking of the 40 plies of the preform of the vane, with drop-offs management.	58
Figure 44: Temperature ramp for the curing phase of the composite vane.....	60
Figure 45: RTM process simulation and main results of the composite vane manufacturing.....	63

LIST OF TABLES

Table 1: Example of the data shared initially in the txt file.....	12
Table 2: Example of the data added from ADDPath® simulation to the txt file.	12
Table 3: Example of the lperm file updated with permeability information of each PAM-RTM® element.	12
Table 4: Performance parallelization trial.	32
Table 5: Definition of POCs and tasks for the development of digital twins and numerical physical workflow.....	48

1 INTRODUCTION

The aim of the CAELESTIS project is to create an innovative, comprehensive Interoperable Simulation Ecosystem (ISE) that seamlessly integrates product design, distributed engineering teams (DET), and manufacturing specialists. This ecosystem seeks to expedite the design and engineering refinement of groundbreaking aircraft for the future. A pivotal aspect of CAELESTIS is its provision of high-fidelity, model-based digital twins, enabling precise predictions at various stages of the product development cycle. This cycle encompasses processes such as automated fiber placement (AFP), laser powder bed fusion (L-PBF), resin transfer molding (RTM), component assembly, and mechanical assessments to determine the product's structural performance.

Within the context of manufacturing processes, there is a pressing need not only to minimize uncertainties at each stage and reduce the number of defective parts but also to guide the design of new components with a holistic focus on both manufacturing and mechanical performance throughout all stages. Consequently, the initial phases of design and manufacturing are expedited in pursuit of a component that considers all mechanical and manufacturing requirements, including the unavoidable defects that may arise during various stages such as AFP, L-PBF, RTM, assembly, and mechanical testing. This acceleration is made feasible through the execution of extensive simulation campaigns, involving a multitude of design and manufacturing scenarios across the entire chain of manufacturing and mechanical performance. Utilizing High-Performance Computing (HPC) resources enables realistic time scales, providing faster and more accurate insights for optimizing both product and process within the manufacturing chain. This approach delivers rapid and precise predictive insights across various design and manufacturing scenarios, offering a comprehensive array of outputs related to mechanical performance, manufacturability, sensitivity analysis and uncertainty quantification.

This deliverable specifically focusses on the RTM and PBF Digital Twins employed in CAELESTIS project for the manufacturing simulations. The modelling strategy for each stage, along with

the overarching workflow of the manufacturing chain developed in the CAELESTIS use case (fan outlet guide vane (FOGV)), is elucidated. Importantly, this modelling strategy is not limited to simulating the FOGV but is also applicable to any component manufactured using AFP, L-PBF, RTM processes.

This deliverable elaborates on the meso-scale strategy developed to predict void generation behavior during RTM process simulations, incorporating bi-phasic computational fluid dynamics (CFD) simulations of the filling stage with detailed tows and gaps geometries. Additionally, PBF analysis of the metallic insert located at the ends of the FOGV is included, starting with the original design that does not initially leverage the benefits of the PBF process. Finally, RTM process models are explained from input data through filling, curing and distortion analysis, showing preliminary results as demonstrator.

Therefore, this deliverable is structured as follows: Section 2 outlines the overall workflow of the CAELESTIS simulations and contextualizes the RTM and PBF processes within this framework; Section 3 presents multiscale models aimed at understanding voids generation to feed RTM simulations; Section 4 describes L-PBF models of the metallic inserts for the FOGV; Section 5 presents RTM models of simplified geometry (proof of concept 1) and preliminary FOGV geometry; and finally, Section 6 summarizes the conclusions and outlines future work to be developed during the extension of work package 4.

2 RTM DIGITAL TWIN IN THE GLOBAL WORKFLOW

The objective of the WP4 is to develop a high-fidelity manufacturing process digital twins including several manufacturing steps, AFP, L-PBF, RTM, and assembly, to enable predictive capabilities across a manufacturing chain. This includes to develop and link Multiphysics models in the manufacturing simulation workflow accounting for singularities and defects propagation during the whole manufacturing steps.

Figure 1 shows the global process workflow defined and built in the WP4, connecting all the models from different simulation software that digitalize the manufacturing chain of the process defined in CAELESTIS for the FOGV use case.

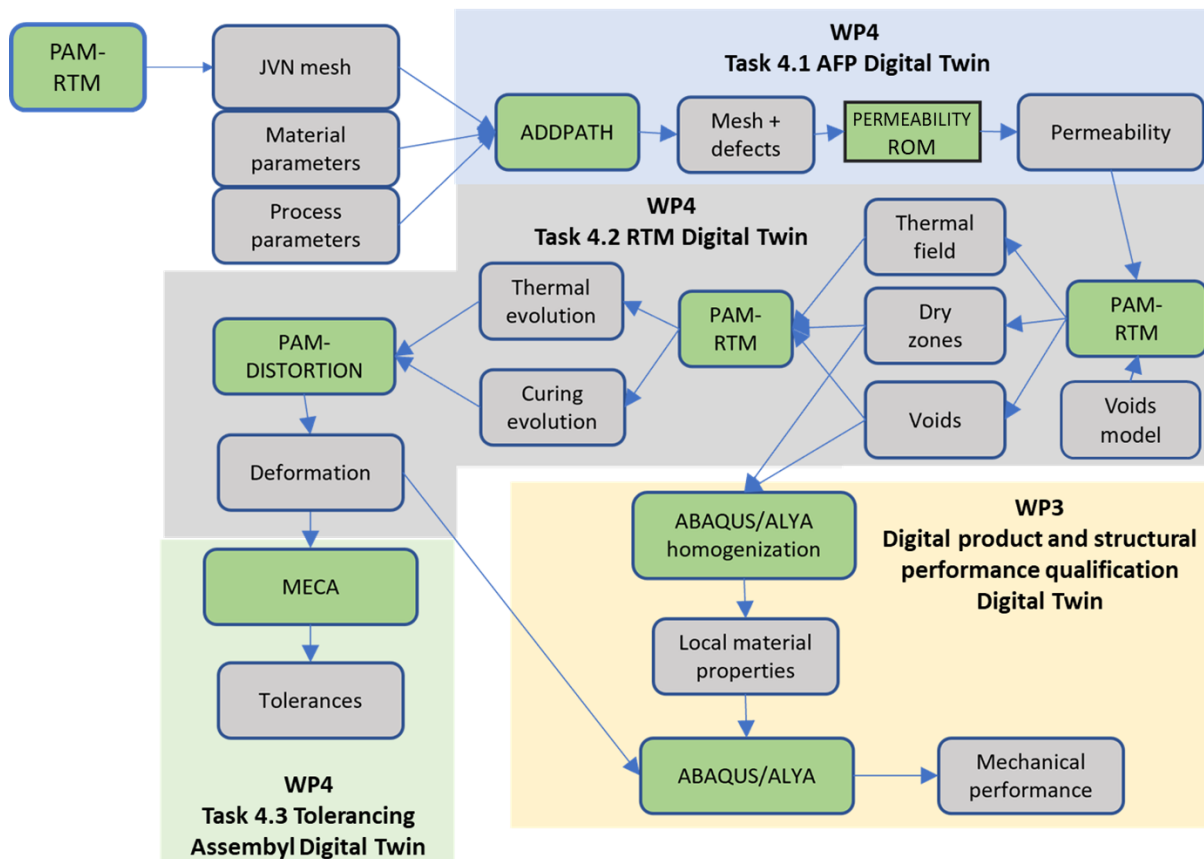


Figure 1: Numerical workflow for processes digital twins.

Task 4.1 develops the simulations of the AFP process and assigns permeabilities for the RTM simulation based on the AFP outputs. ADDPath® software plans and simulates the deposition sequence of the fibers, providing preform layup and defects generations, such as misalignment, gaps and overlaps. The permeability assignment for the RTM process is done evaluating a Reduced Order Model (ROM) with the cloud of points that ADDPath® evaluates and enriches with additional information of the tows and defects. The ROM is based on CFD simulations in Alya® with parametrized representative geometries (see deliverable D4.1 for detailed information of this stage).

Task 4.2 efforts are directed towards RTM process including filling, predictive models for void generation, curing and demolding stages of RTM, and L-PBF process. Voids generation models during RTM are based on bi-phasic CFD simulations, accounting for resin advance towards air, tows and resin material properties, and flow conditions. RTM process models and the demolding of composite parts is being developed, utilizing PAM-RTM[®] and PAM-DISTORTION[®] software alongside AFP inputs, regardless of defects presence. Additionally, Task 4.2 involves the development of a dedicated model based on the ESI-AM[®] software for the L-PBF process of titanium fixing parts.

Task 4.3 aims to establish a virtual "coordinate measuring machine" capable of automatically estimating tolerances on composite parts from distortions of virtual surfaces of composite parts and to analyze their impacts on the tolerancing analysis of the assembly of the composite part and metallic parts of the OGV, with MECAMaster[®] software (see deliverable D4.3 for detailed information of this stage).

Thus, this workflow aims to connect all the digital twins of manufacturing processes, integrating the permeability field, defects and layup orientation, void generation, and shape distortions.

Two of the main objectives of CAELESTIS project are:

- to develop a numerical workflow between processes digital twins,
- to propagate processes defects in the numerical workflow.

To build the numerical workflow between the different digital twins dedicated to each process of the manufacturing of the complete OGV, with the exchange of numerical and physical data, as input / output parameters, Python[®] scripts and intern development in some software have been developed, based and using the API of the different software.

For the workflow between AFP and RTM processes simulations, two dedicated numerical files, the lperm file and a txt file, have been created, which will be used and completed at each step of the digital thread. The steps are shown in Figure 2 and detailed in the following points:

- 1° initial generation of the lperm file, by PAM-RTM® with the meshing data,
- 2° calculation of the centroid of each finite element of the meshing, with its coordinates with Python® script and integration of the data in the txt file. Table 1 shows an example of the initial data of the txt file,
- 3° integration of the orientation and the local reference axes data for each ply of the preform at the centroid location, coming from ADDPath®, and integration of data in the txt file,
- 4° integration of the potential AFP process defects, misalignments, gaps and/or overlaps data for each ply of the preform, with the locations and the dimensions of the defects, at the centroid location, coming from ADDPath®, and integration of data in the txt file. Table 2 shows an example of the updated data of the txt file,
- 5° evaluation of the data from txt file and integration of the permeabilities values, coming from surrogate model, with defects consideration, and integration of data in the lperm file,
- 6° the completed lperm file, with all the previous information is the used in PAM-RTM® for the filling simulation. The effect of the occurrence of defects in the preform is considered by the variations of the permeabilities values. Table 3 shows an example of the final lperm file.

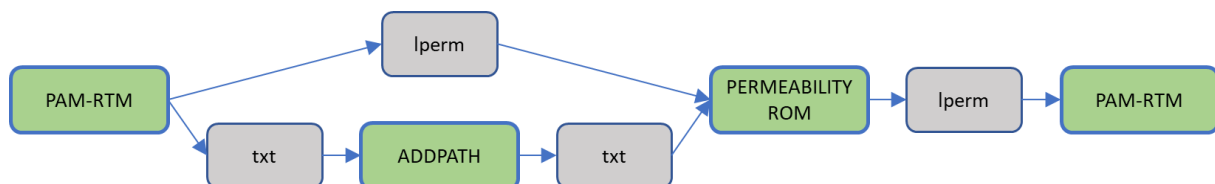


Figure 2: Numerical and physical data exchanged between ADDPath®, permeability ROM and PAM-RTM®.

ID	Coordinates		
3457	147.5	77.5	1.95
3458	150.0	77.5	1.85
...

Table 1: Example of the data shared initially in the txt file.

Layer Number	Ply Orientation	Normal	0° Layer Orientation	Distance	
1	0,0,0,0,0,0,0,0,0,0	0,0,-1	1,0,0	1.95	
1	0,0,0,0,0,0,0,0,0,0	0,0,-1	1,0,0	1.85	
...	
Gap	Gap Distance	Gap Size	Overlap	Overlap Distance	Overlap Size
-1	9999	9999	-1	9999	9999
-1	9999	9999	-1	9999	9999
...

Table 2: Example of the data added from ADDPath® simulation to the txt file.

ID	Thickness	Fiber Content	K1	K2	K3
3457	0.00018	0.55	1.42e-09	5.75e-13	6.04e-13
3458	0.00018	0.55	1.42e-09	5.75e-13	6.04e-13
...
Perm_Vec1_x	Perm_Vec1_y	Perm_Vec1_z	Perm_Vec2_x	Perm_Vec2_y	Perm_Vec2_z
0	1	0	0.9368	0	-0.3498
0	1	0	0.93413	0	-0.3376
...

Table 3: Example of the lperm file updated with permeability information of each PAM-RTM® element.

For the workflow connection between voids and RTM models, PAM-RTM® simulation software incorporates the possibility to be fed by a model that relates resin and flow conditions to the occurrence of voids inter-tows and intra-tows. Therefore, the results of the two-phase mesoscale CFD simulations are directly incorporated into the RTM simulation using the tool

already incorporated in PAM-RTM®. In the RTM step, the fixing parts, manufactured by L-PBF, are considered as boundary conditions in filling phase simulation.

Finally, for the workflow between RTM and tolerancing assembly processes simulations, a Python® script has been developed to:

- automatically extract the nodes coordinates of the non-deformed and deformed meshes (with demolding distortions data) to estimate the tolerances on the composite parts,
- calculate the tolerancing KPI of the geometrical functional requirements defined on the assembly (of POC1 and OGV), with surrogate linear model, coming from MECAmaster® software.

The fixing parts, manufactured by L-PBF, with their CADs and the tolerances on their geometrical features, are integrated in the assembly of the OGV in the MECAmaster® model. The shape distortions of the parts are estimated by simulations on ESI-AM® software.

Thus, we have developed a seamless workflow between AFP, L-PBF, RTM and assembly simulations that allows us to simulate in an automated way the complete manufacturing process including defects generated in AFP and their propagation and effect on permeability, RTM (including voids), deformation and assembly.

3 MULTISCALE VOIDS MODEL

Void formation represents a critical challenge in composite manufacturing, as these imperfections can significantly compromise the mechanical properties and structural integrity of the final product. The complexity of predicting voids in RTM is further magnified by its inherently multiscale nature. This complexity arises from multiple mechanisms governing void formation and transport, operating across various scales from the microscopic to the macroscopic. Factors such as resin flow dynamics, fiber arrangement, and interaction between different resin-air phases play pivotal roles in determining void formation, each contributing

to the intricate mosaic of processes that culminate in voids. Given this multifaceted and multiscale interplay, predicting their occurrence with precision remains a complex endeavor. The strategy adopted to computationally study the voids generation consists in developing Representative Volume Elements (RVEs) at the meso-scale level and exploring through Computational Fluid Dynamic (CFD) simulations. These simulations aim to establish a comprehensive model that correlates flow conditions with voids formation both inter- and intra-tows. By dissecting the biphasic nature of the flow and the underlying physics at multiple scales, the multiscale voids model endeavors to provide insights into the intricate interplay between flow conditions and void formation. Understanding this complexity is crucial for advancing our understanding and enhancing the predictability of voids in AFP-assisted RTM processes.

Unlike woven fabrics, AFP-assisted RTM presents unique challenges and characteristics (see **Figure 3**). In this process, free channels exist between the tows, allowing the resin to flow more easily compared to the interior of the tows. Within these tows, despite the fibers being preferentially aligned in the deposition direction, permeabilities are significantly low. Additionally, at the microscale, a phenomenon distinct from higher scales emerges, capillary pressure. This capillary pressure promotes resin advancement by acting on the resin's free surface, influenced by material properties such as the resin-fiber contact angle and surface tension. Consequently, the disparity in resin front progression within the tows versus between the tows (channels) is determined by the interplay of permeability and capillary pressure values under varying process conditions. These differences can significantly influence void formation, highlighting the intricate dynamics at play in AFP-assisted RTM processes.

Therefore, bi-phasic CFD models of RVEs at the meso-scale are being developed. These models incorporate the capillary pressure within the tows, and different flow conditions are imposed to assess resin filling both intra- and inter-tows, as well as void generation. All simulations are conducted using the well-established open-source software OpenFOAM®.

3.1 Meshing

The geometry of the RVE is generated using the same dimensions and methods as the permeability RVE models described in Deliverable 4.1. However, different meshing strategies have been explored for the two-phase models. To test the meshing approaches, three meshes are generated using a simple geometry of one layer of fibers with an orientation of 45° and different elements: hex-dominant, tetrahedral and voxels.

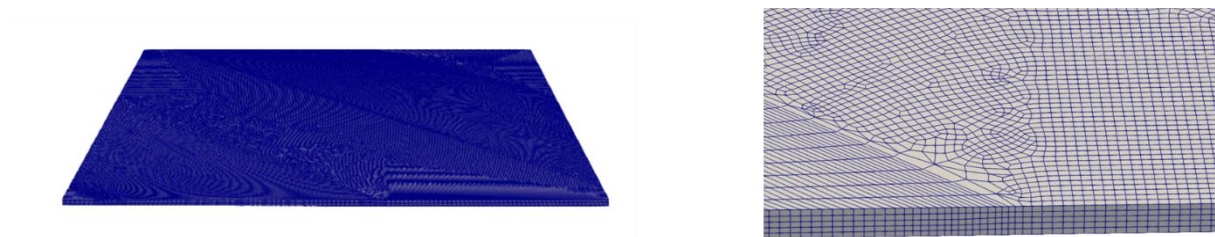


Figure 5: Mesh of hexahedral elements (full domain and detail).

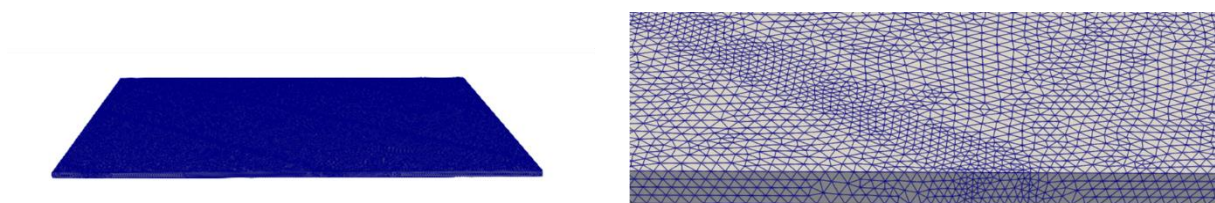


Figure 6: Mesh of tetrahedral elements (full domain and detail).

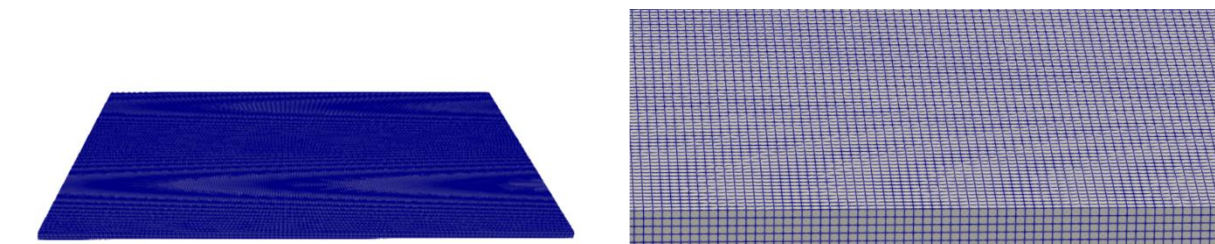


Figure 7: Mesh of voxels elements (full domain and detail).

The meshes were tested for a simple simulation of single-phase flow, allowing to compare the different meshing approaches in terms of stability, accuracy and computational time.

Finally, voxel elements were employed to streamline mesh generation and leverage the advantages of these elements in Volume of Fluid (VOF) simulations, such as OpenFOAM®. Interestingly, simulations conducted using this mesh type not only exhibited no mesh-related issues but also demonstrated accelerated convergence speeds.

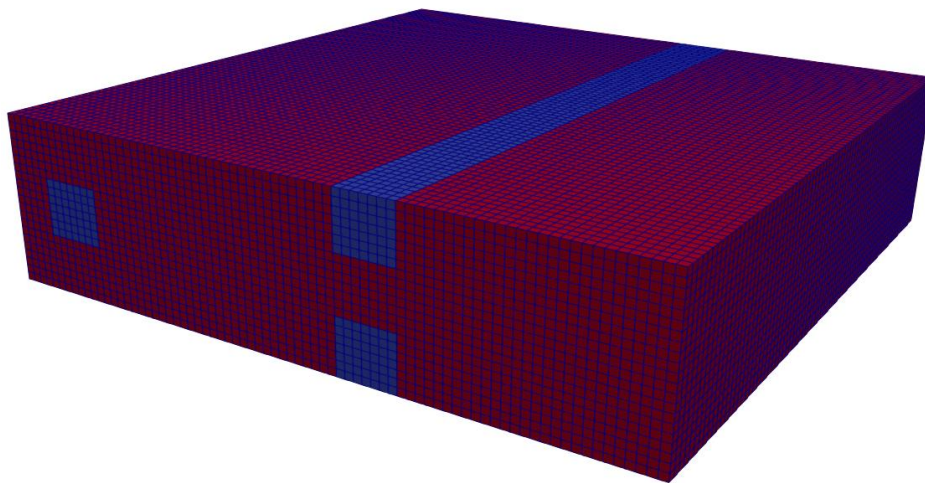


Figure 8: Mesh of voxels elements with three layers of fibers. Orientation 0 degrees.

To further optimize the modeling process, a mesh sensitivity analysis was also conducted to determine the optimal element resolution for the models. To do that, three meshes were generated using voxels elements and increasing the number of elements in height (Z-axis).

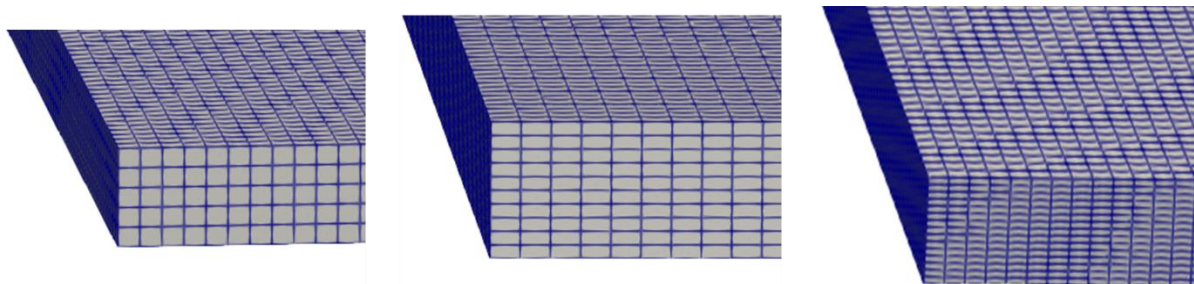


Figure 9: Mesh of voxels elements with increasing number of elements in Z (5, 10, and 15).

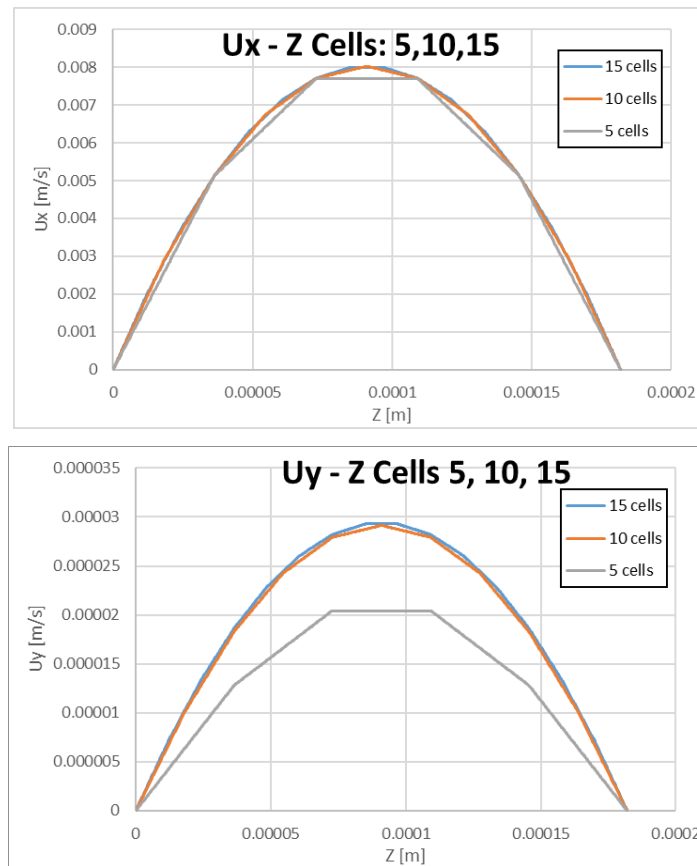


Figure 10: Comparison of velocity profiles in X and Y for meshes with increasing number of elements in Z direction.

The optimal number of cells in Z-axis is 10 elements. It is observed that with only 5 elements, the velocity profiles are not accurate enough; on the other hand, increasing the number of elements from 10 to 15 does not improve the resolution of the velocity profile, but the computational time is increased accordingly. Thus, 10 elements provide the best trade-off in terms of accuracy and computational cost.

Consequently, an in-house Python® script was developed to automate the generation of voxel meshes and all requisite OpenFOAM® setup files. This approach was ultimately chosen as the preferred meshing strategy due to its efficiency in model generation, reliability and convergency.

3.2 Case configuration

This section provides a thorough description of the setup for the CFD simulation focused on the resin injection in an RTM process. It includes the development of the appropriate solver, the strategy for simulation and the specific case configurations, including boundary conditions and the numerical characterization of porous media.

First trials

Aiming at identifying a suitable solver for the simulation of resin injection, the official documentation of OpenFOAM® related to simulation of porous media flow was reviewed. To be able to accurately represent the process, the appropriate solver had to include a combination of specific features. These requirements involved the simulation of multiphase flows and the adaptability of both porous and non-porous zones within the fluid domain.

The exploration through the range of solver options in OpenFOAM's documentation led to the selection of interFOAM solver with an explicit porosity source term as initial simulation approach.

The interFOAM solver is specifically designed for the simulation of two immiscible fluids with interface tracking through the Volume of Fluid (VoF) method. The explicit treatment of porosity is implemented using the `explicitPorositySource` class with DarcyForchheimer coefficients, that can be applied restrictively to the defined porous zones and that has the capability to model anisotropic media.

However, the selected approach failed to provide the expected results. The `explicitPorositySource` applied a penalty to the porous zones in the form of sink term in the momentum equation, which resulted in a lower velocity in the fibers. However, the velocity at the interphase between the free fluid and the porous media was not coupled and there was no transition between the fibers and the inter-tow channels.

Additionally, this methodology did not account for the fluid porosity inside the fibers or the capillary pressure effects. Thus, once the preliminary results were analyzed, it was concluded that this approach did not provide a satisfactory or realistic approach of the resin injection in RTM processes.

Solvers

The results of the CFD simulation of resin injection using an approach based solely on OpenFOAM's official documentation proved insufficient to provide a realistic representation of the process. Consequently, further exploration was necessary to seek alternatives from supplementary bibliographical sources.

Through this search, the solver `hybridPorousInterFoam`³ stood out, showing several characteristics aligned with the requirements of the simulation. This solver is specifically designed for simulating multiphase flows in porous media in hybrid domain, with special focus in practical applications related to hydrogeology, like groundwater flow or oil reservoirs modelling.

Built upon the `interFoam` solver, `hybridPorousInterFoam` inherits its capability for multiphase simulation with interface capturing schemes, making it suitable for modelling the flow of two immiscible fluids with well-defined interfaces. In this solver, the momentum equation is modified to include the fluid porosity and an additional drag force term that represents the Darcy term.

A dual scale approach is considered to resolve both characteristics length scale present in the computational domain: a small-scale porous zone, where the flow is solved adding the Darcy's Law, and large-scale free-fluid zone, solved with Navier-Stokes equations. The coupling between both scales is achieved by preserving mass conservation and continuity of stresses

³ Carrillo, F. J., Bourg, I. C., & Soulaine, C. (2020). Multiphase flow modeling in multiscale porous media: an open-source micro-continuum approach. *Journal of Computational Physics*: X, 8, 100073.

at the porous interface. Unlike the previous approach, the flow behavior at the interface between the porous media and the free fluid is accurately represented, allowing a smooth transition between the two domains.

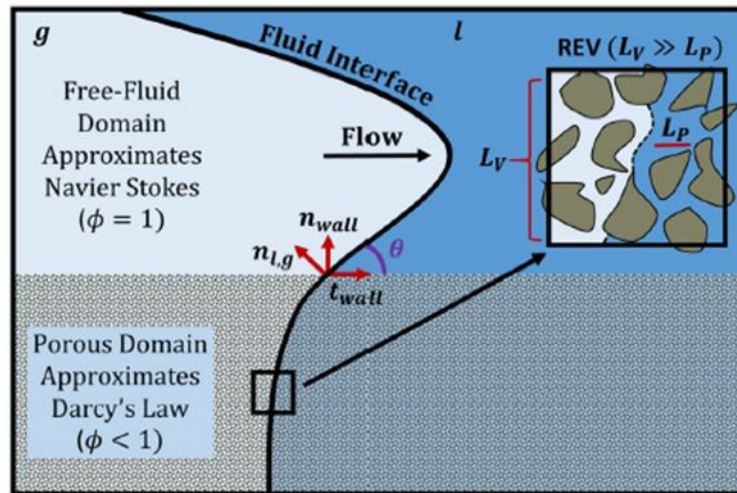


Figure 11: Representation of the hybridPorousInterFoam approach for the simulation of multiphase flow in hybrid porous media³.

Additionally, the solver incorporates the determination of the capillary pressure and its integration into the solver equations, accounting for the effects of surface tension and fluid-fluid interaction within the porous domain. Currently, the implemented capillary pressure models (Brooks and Corey⁴ and Van Genuchten⁵) are specific for the characterization of capillary effects in soil water dynamics.

Thus, a thorough analysis of hybridPorousInterFoam solver concluded that it possessed most of the required features; however, certain essential functionalities were missed. First, the permeability characterization was restricted to isotropic porous media, while the fibers exhibited an anisotropic structure. On the other hand, the capillary pressure approximations available in the solver were not suitable for the modelling of capillary effects in fibers.

⁴ R. Brooks, A. Corey, Hydraulic properties of porous media, Hydro Paper 3, Colorado State University, 1964, p.27.

⁵ M.T. van Genuchten, A closed-form equation for predicting the hydraulic conductivity of unsaturated soils, Soil Sci. Soc. Am. J. 44(5) (1980) 892–898.

Consequently, it was necessary to expand the capabilities of the current solver to meet the requirements of the simulation.

In `hybridPorousInterFoam`, the drag force was determined as the product of viscosity and inverse permeability. For an isotropic medium, permeability was a constant value and consequently, so was the drag force term in the momentum equation. However, to model permeability in anisotropic media, a permeability tensor was needed. As a result, the code was adjusted to be able to read and handle the permeability as tensor, as well as transform the derived variables accordingly.

Further modifications were proposed and implemented to address certain restrictions regarding numerical methods. For the discretization of source or sink terms in the momentum equation, OpenFOAM® provided a function (`fvm::Sp`) where the term was managed with an implicit method. This was the implementation approach of `hybridPorousInterFoam` solver, where the drag force was introduced in the momentum equation as `fvm::Sp(Drag, U)`. However, this function did not accept a tensor as coefficient, so the updated Drag force in tensor form could not be straightforwardly implemented implicitly. An alternative approach could be to formulate the term explicitly, but the explicit treatments were more unstable compared to implicit treatments. Explicit methods often require smaller time steps to maintain numerical stability, making them computationally more expensive, while implicit methods offer greater stability and can handle larger time steps. Given the exceptionally low permeability of the porous media in this case, where typical values of fiber permeability were around $1e-13 \text{ m}^2$ to $1e-14 \text{ m}^2$, the resulting drag term was significantly high, differing by several orders of magnitude from other terms in the momentum equation. Consequently, the numerical instability associated with explicit treatment was further exacerbated by this issue.

The solution was to decompose the permeability tensor into two terms, one of which was a diagonal matrix where all its diagonal elements had the same value, corresponding to the

average of the elements of the original tensor (Equation 1 to Equation 5). This diagonal matrix was also the product of a scalar and the identity matrix (\mathbf{I}).

$$K^{loc} = \begin{pmatrix} K^{long} & 0 & 0 \\ 0 & K^{trans} & 0 \\ 0 & 0 & K^{trans} \end{pmatrix}$$

Equation 1: Permeability tensor in local orientation.

$$K^{glob} = AK^{loc}A^T$$

Equation 2: Local to global transformation of the permeability tensor.

$$Drag = \frac{1}{K^{glob}}$$

Equation 3: Permeability to Drag conversion.

$$Drag^{iso} = \left(\frac{\sum_{i=1}^3 \sum_{j=1}^3 Drag_{ij}}{3 \cdot 3} \right) \times \mathbf{I}$$

Equation 4: Isotropic drag tensor.

$$Drag^{aniso} = Drag - Drag^{iso}$$

Equation 5: Anisotropic drag tensor.

Therefore, the second term of the decomposition ($Drag^{iso}$) was suitable for its implementation in the momentum equation with an implicit treatment and the stability of the solver was significantly increased.

The anisotropic nature of the fibers also impacted the modelling of the capillary pressure in this case of porous media. Specifically, longitudinal (Equation 6) and transversal (Equation 7) capillary pressure⁶ exhibited different behaviors and different expression were required to be adequately represented:

⁶ Dungan, F. D., & Sastry, A. M. (2002). Saturated and unsaturated polymer flows: microphenomena and modeling. *Journal of composite materials*, 36(13), 1581-1603.

$$P_c^{long} = \frac{2 \cdot \gamma \cdot \cos(\theta)}{r_f \cdot \varepsilon} (1 - \varepsilon)$$

Equation 6: Capillary pressure in longitudinal direction of the fibers.

$$P_c^{trans} = \frac{\gamma \cdot \cos(\theta) \cdot (1 - \varepsilon)}{r_f \cdot \varepsilon}$$

Equation 7: Capillary pressure in transversal direction of the fibers.

where γ was the surface tension of the resin, θ is the resin-fiber contact angle, r_f was the fiber radius, and ε was the porosity.

Thus, the capillary effects were described at macroscopic scale by a capillary tensor σ_{cap} , having the same eigen-directions as the permeability tensor:

$$\sigma_{cap}^{local} = \begin{pmatrix} P_c^{long} & 0 & 0 \\ 0 & P_c^{trans} & 0 \\ 0 & 0 & P_c^{trans} \end{pmatrix}$$

Equation 8: Definition of diagonal capillary tensor.

and then transforming from local to global coordinates depending on the orientation generated in the RVE generator, similarly to permeability:

$$\sigma_{cap}^{global} = A \sigma_{cap}^{local} A^T$$

Equation 9: Definition of oriented capillary tensor.

Capillary effects led to an increase in pressure at the resin-air interface, denoted as p_{cap} and expressed as:

$$p_{cap} = n \cdot \sigma_{cap}^{local} \cdot n$$

Equation 10: Definition of capillary pressure.

where n is the normal vector to the resin-air interface.

In the new version of the solver, the code was modified to enable the reading of the capillary tensor (Equation 9) from the case set-up and subsequently calculated the capillary pressure using Equation 10. Thus, the capillary models available in `hybridPorousInterFoam` were replaced by a new formulation that better aligned with the representation of the physics of

resin injection, while the implementation of the capillary pressure term in the solver equations remained unaltered.

Following the described modifications, the result was a new solver that was able to accurately simulate a biphasic transient flow over a heterogeneous anisotropic porous media.

The initial `hybridPorousInterFoam` solver also included a simplified version based on `pimpleFoam` solver instead of `interFoam`, that can be used to model single-phase flow in hybrid scale porous media. This solver was also adapted to the particularities of the resin injection case including the same implementation of anisotropic treatment of porous media that was described above, while the consideration of capillary pressure modelling is only required in the context of multiphasic flows.

With the completion of the solver development for the CFD model of biphasic flow in hybrid anisotropic porous media, a comprehensive simulation tool is available to accurately capture the relevant physical phenomena involved in resin injection.

Simulation strategy

Following the definition of the meshing approach and the development of the solver, the next step was to formulate a strategy for the simulation of resin injection that can be applied to a given RVE mesh. The aim of this methodology was to ensure that the simulation process runs in a structured and efficient manner while achieving accurate results. This is essential to establish a simulation workflow that is able to run from geometry definition to results generation, ensuring that the designed cases are generated, executed and postprocessed automatically.

The simulation strategy consisted of two steps. The first step was the simulation of monophasic fluid flow over the RVE mesh. Once this simulation is converged, the velocity profiles were extracted and imposed as boundary conditions at the inlet of the second simulation, the biphasic flow using the same RVE mesh.

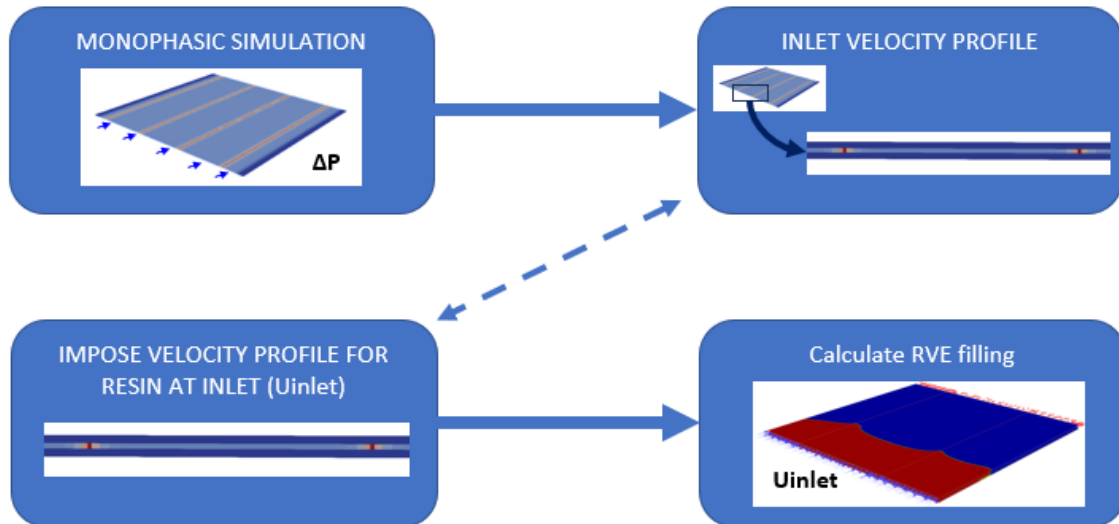


Figure 12: CFD simulation of voids: simulation strategy imposing pressure drop in the monophasic simulation (ΔP) and velocity at the inlet (U_{inlet}).

This second phase represents the resin flow injection, but performing the monophasic simulation as case initialization is necessary to determine realistic velocity profiles at inlet. The combination of velocity at inlet and pressure at outlet is often considered of the most robust sets of boundary conditions and helps stabilize the simulation, especially when the flow field is complex, such as in a multiphasic simulation.

Next, the configuration of each CFD simulation is described in detail.

First step: monophasic simulation

During the simulation of single-phase flow, the resin dynamics in a heterogeneous porous media were calculated, representing the injected flow in a part of the mold that is already filled. The aim is to obtain a realistic velocity profile at the inlet of the domain for the initialization of the biphasic simulation.

A representative domain is depicted in Figure 13 to illustrate the generic boundary definition of the case. In Z-axis, named Top and Bottom, no-slip wall conditions were applied, while Y-axis were set as cyclic, to account for the domain periodicity. Inlet and outlet were located in

X-negative and X-positive axis respectively. For the configuration of the monophasic simulation, a fixed pressure drop between inlet and outlet was set, while the velocity gradient at the inlet and the outlet is set to zero. These boundaries are defined accordingly to any geometry, regardless of the domain length or the number or orientation of layers of fibers.

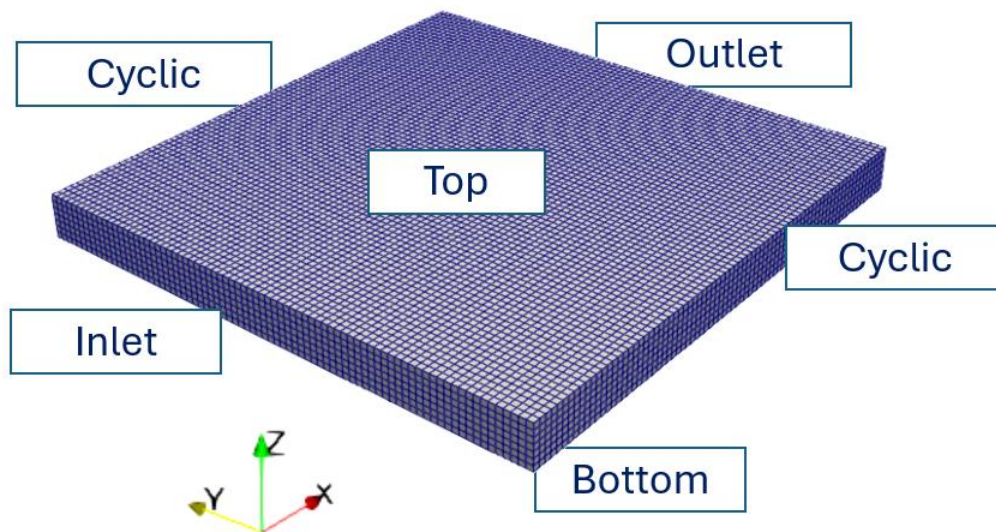


Figure 13: CFD simulation of voids: boundary conditions.

The flow was set to laminar, the viscosity was considered Newtonian, and set constant to the dynamic viscosity of the resin. From the definition of the fibers and matrix zone during the meshing phase, the porous field was characterized. In the zones identified as fibers the solid indicator was set to 1, while the fluid porosity and permeability tensor were defined according to the textile specifications. In the case of the permeability tensor, the correct definition was the global permeability tensor, that included the fiber orientation. Therefore, if the orientation of the layers was different, the corresponding global permeability tensor must be provided for each one. The porous media definition is represented in **Figure 14: CFD simulation of voids: porous media definition**: the solid indicator (Solid), fluid porosity (ϵ) and permeability magnitude (K), for a simple RVE geometry with one layer of two fibers and one fluid channel.

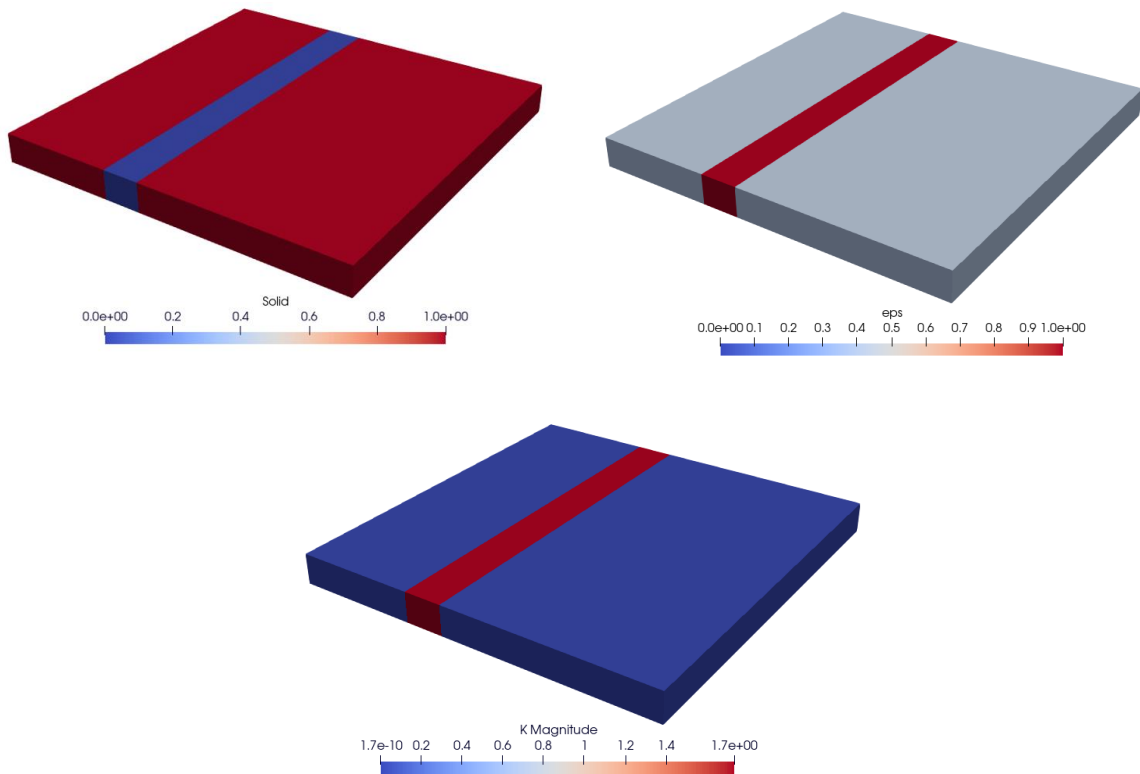


Figure 14: CFD simulation of voids: porous media definition (solid indicator, porosity and permeability)

The result of this simulation was the determination of the velocity and pressure fields, as depicted in Figure 15: CFD simulation of voids: single-phase velocity and pressure fields. The test geometry of one layer and two fibers as test case.

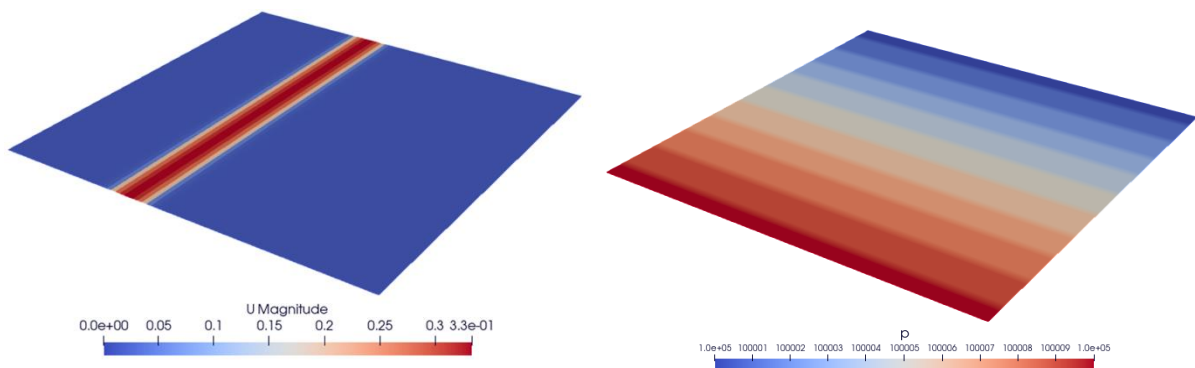


Figure 15: CFD simulation of voids: single-phase velocity and pressure fields.

Second step: biphasic simulation

The next step is to run the biphasic simulation that represents the injection of the resin into a fraction of the mold over the dry fibers. The boundary conditions and the porous media definition are set similarly to the monophasic case with small changes (see Figure 16).

In this case, the boundary conditions at inlet are set to fixed non-uniform velocity, obtained from the velocity profiles determined in the single-phase flow. The outlet is set to fixed pressure, specifically to the ambient value.

Additionally, the phase fractions must be defined. The resin fraction is set to 1 at inlet and the case is initialized with a small fraction of the domain already filled at the domain inlet.

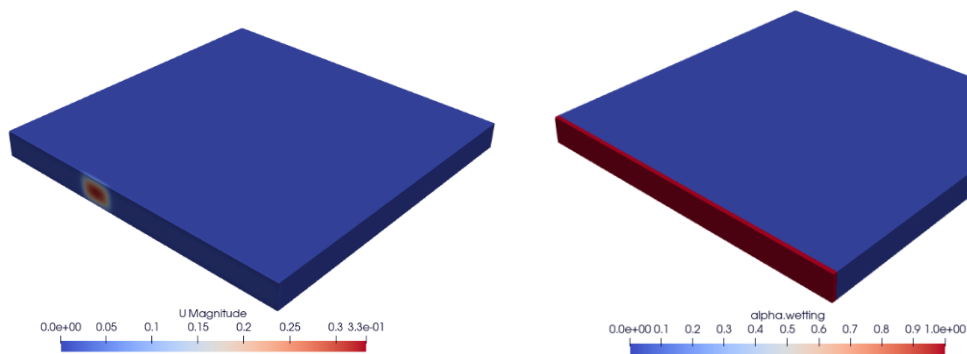


Figure 16: CFD simulation of voids: initialization of biphasic simulation.

To complete the characterization of the porous media, the capillary pressure is provided in the form of the oriented capillary pressure tensor (see Equation 9).

Once the simulation case is running, the evolution of the volumetric average of resin fraction in the domain, in the free fluid and the fibers are separately monitored, as well as the pressure at inlet. At the end of the simulation, these reports will provide the final value of air content, micro and macro voids, and final injection pressure.

Due to the characteristics of the simulation (multiphasic fluid flow in hybrid porous media), the computational cost is significant. At the time, these cases are running for different capillary numbers and the outcome will serve as data points for the fitting of the micro-macro voids curve depicted in **Figure 4**.

3.3 Workflow and HPC

The simulation strategy outlined in section 3.2 has been integrated into a workflow where inputs for geometric, material, and flow conditions are selected. Subsequently, the necessary geometry, mesh, and OpenFOAM® files for conducting both single-phase and two-phase simulations are automatically generated. This workflow is built upon in-house Python® scripts developed in Task 4.1 (for more details, refer to Deliverable 4.1). These scripts automatically generate an RVE geometry based on parameters such as tow dimensions, orientations, distance between tows, or final fiber volume fraction, among others (see **Figure 17**).

While the mesh discretization process and the assignment of orientation and properties to each element remain consistent with those used in Task 4.1, OpenFOAM® requires a specific mesh file format and numbering. As a result, specific Python® scripts have been developed to convert and write the mesh in the required OpenFOAM® format.

Meshes are generated only once for each geometric condition (single-phase and two-phase). Once the mesh files are generated, all material and boundary condition files are written for both single-phase and two-phase simulations, accommodating multiple flow conditions within each geometry. Furthermore, to establish a connection between the single-phase and two-phase simulations, a Python® script has been devised to extract velocities from the input faces and apply them as boundary conditions in the two-phase scenario.

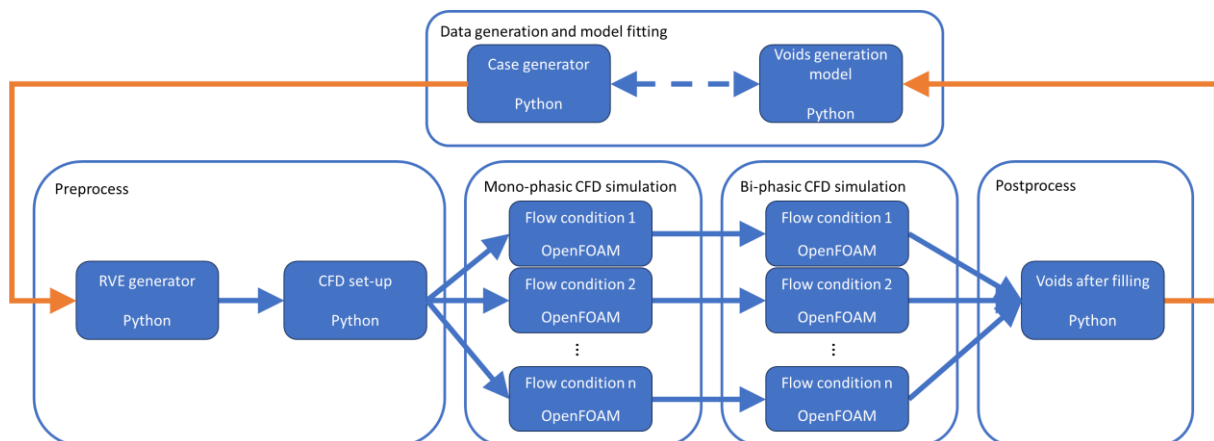


Figure 17: Workflow to generate the voids model.

All simulations are executed on the Nordv3 cluster at the Barcelona Supercomputing Center (BSC) due to the significant computational resources typically required for biphasic simulations. To analyze the computational times and parallelization performance offered by OpenFOAM®, preliminary trials were conducted as follows.

Parallelization performance

The efficiency and performance of computational simulations often depend on the optimization of parallel computing resources. Understanding the limitations and optimal configurations of parallelization can significantly impact the computational speed and accuracy of simulations.

For a given RVE geometry where all the tows are oriented in the same direction and a pressure drop is imposed, an extensive mesh was generated and distributed across varying numbers of CPUs. This trial is conducted in the monophasic simulation since they are much faster than biphasic ones. Table 4 presents the numbers of the parallelization performance study. It reveals a threshold of approximately 4000 elements per CPU. Beyond this point, increasing parallelization proves ineffective, as the computation time cannot be further reduced by simply adding more CPUs.

Parallelization (elements / CPU)	Computational time (min)
~ 62200	5.65
~ 31100	4.88
~ 15500	3.62
~ 7800	3.35
~ 3900	2.33
~ 2000	2.7
~ 1000	9.4

Table 4: Performance parallelization trial.

Computational time

The total computation time of each flow condition is mainly affected by biphasic simulations. The problem with these biphasic simulations is that there are very large speed differences between the zones outside the tow (without porous permeability) and inside the tow (adding the term for permeability). This causes the required time steps to be very small so that the flow does not advance too quickly between one time and the next in the permeability-free zones (especially when the channels generated between the tows are aligned in the flow direction). However, at the same time, the total time needed to fill the entire RVE increases dramatically due to the slow resin velocities inside the tow.

Therefore, an RVE with reduced tow width and number of elements was analyzed in order to study the convergency dependent on the time increment. The RVE had 2mm of tow width and 0.2mm between tows with an element length of approximately 0.03mm (see Figure 18).

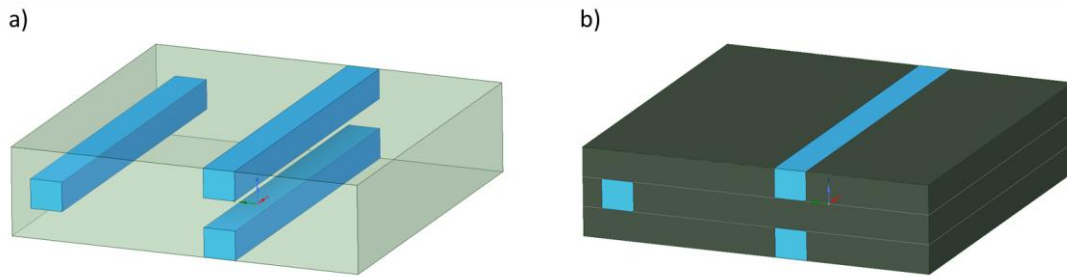


Figure 18: RVE with small tows to analyze the simulations, a) shows the gaps between tows (blue), and b) shows the complete model.

Bi-phasic simulation showed an important sensitivity response to the time increment, resulting in approximately $1e-8$ seconds of optimal time increment.

3.4 First simulations

In this section, some preliminary results of the simulations for studying the increase in time increment are presented (see Figure 18).

For the execution of these simulations, specific material properties for this type of material are required. In addition to properties such as viscosity and density of the resin, and permeability and volume fraction of the tows, the surface tension of the resin with air and the contact angle of the resin with the fibers are also necessary. The viscosity and density properties of the resin are obtained from the supplier's data sheet, and the permeability is calculated based on the volume fraction of each element following Gebart's equation. As in Deliverable 4.1, the volume fraction of each element is calculated in the geometry and mesh generator Python[®] script. However, the surface tension and contact angle properties are not available from the supplier, so bibliographic data is used for the surface tension, and the results obtained experimentally by AIMEN are used for the resin-fiber contact angle.

The first voids simulation is performed with extreme values of resin velocity, showing a significant advancement of the resin inside the channels programmed between tows (see

Figure 19 and Figure 20). This result needs to be further analyzed in conjunction with the rest of the simulations by changing the flow conditions to determine the effect these channels have on the appearance of voids.

Therefore, from the initial studies conducted, two potential risks are observed that need to be studied in more detail: the effect of the channels on void generation and the possibility of accelerating biphasic simulations.

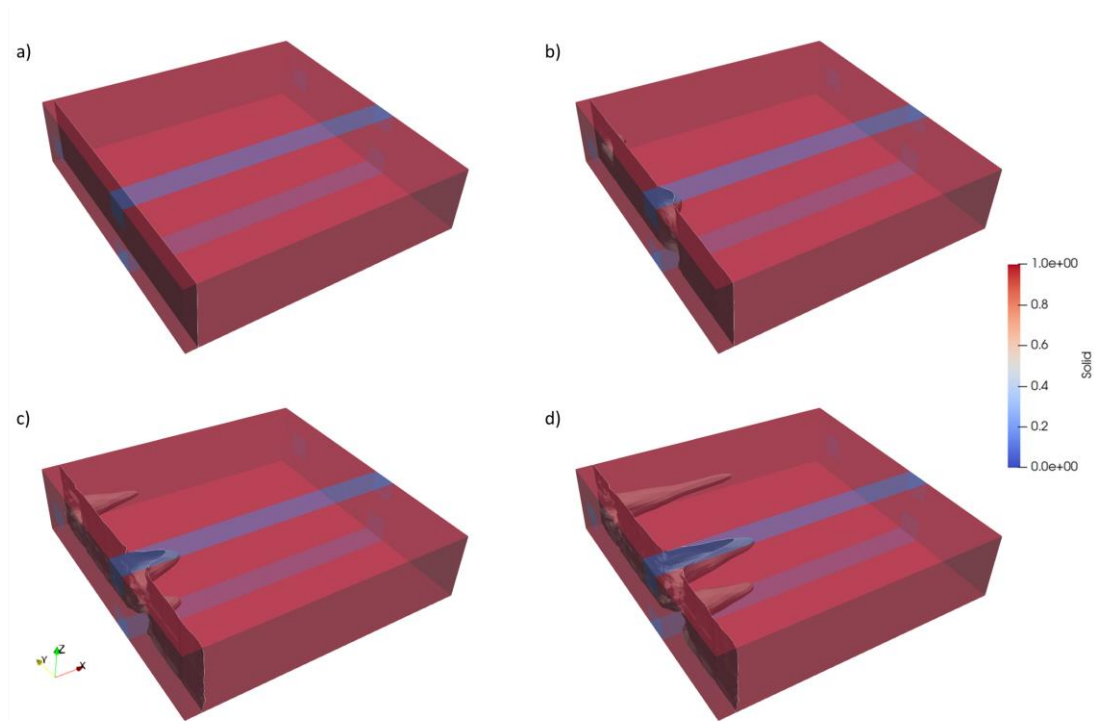


Figure 19: Preliminary results showing gaps (blue) and tows (red) together with the flow front of the resin. a, b, c, and d show four different increasing times. (View 1)

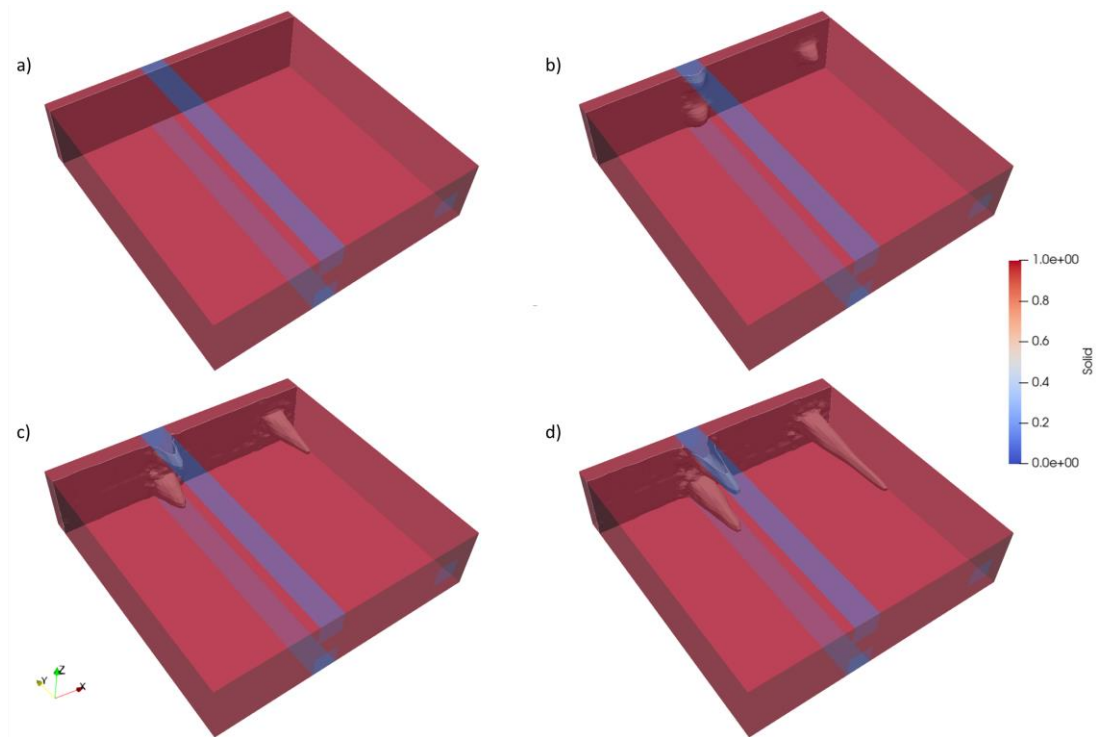


Figure 20: Preliminary results showing gaps (blue) and tows (red) together with the flow front of the resin. a, b, c, and d show four different increasing times. (View 2)

4 L-PBF SIMULATION

The outer and inner metallic blade fittings are foreseen to be manufactured using laser powder bed fusion (L-PBF). The preliminary design of both fittings is shown in Figure 21.

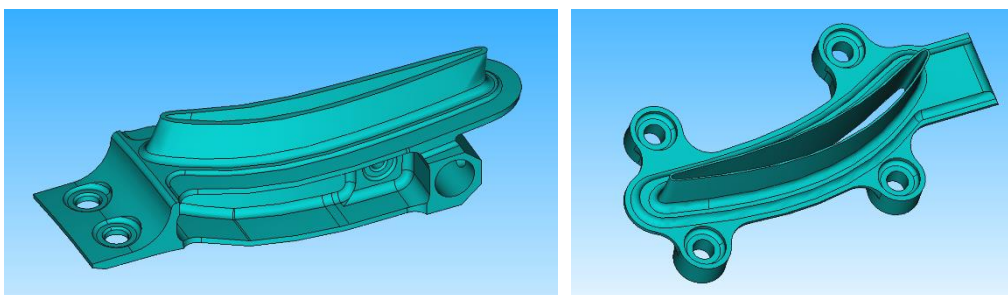


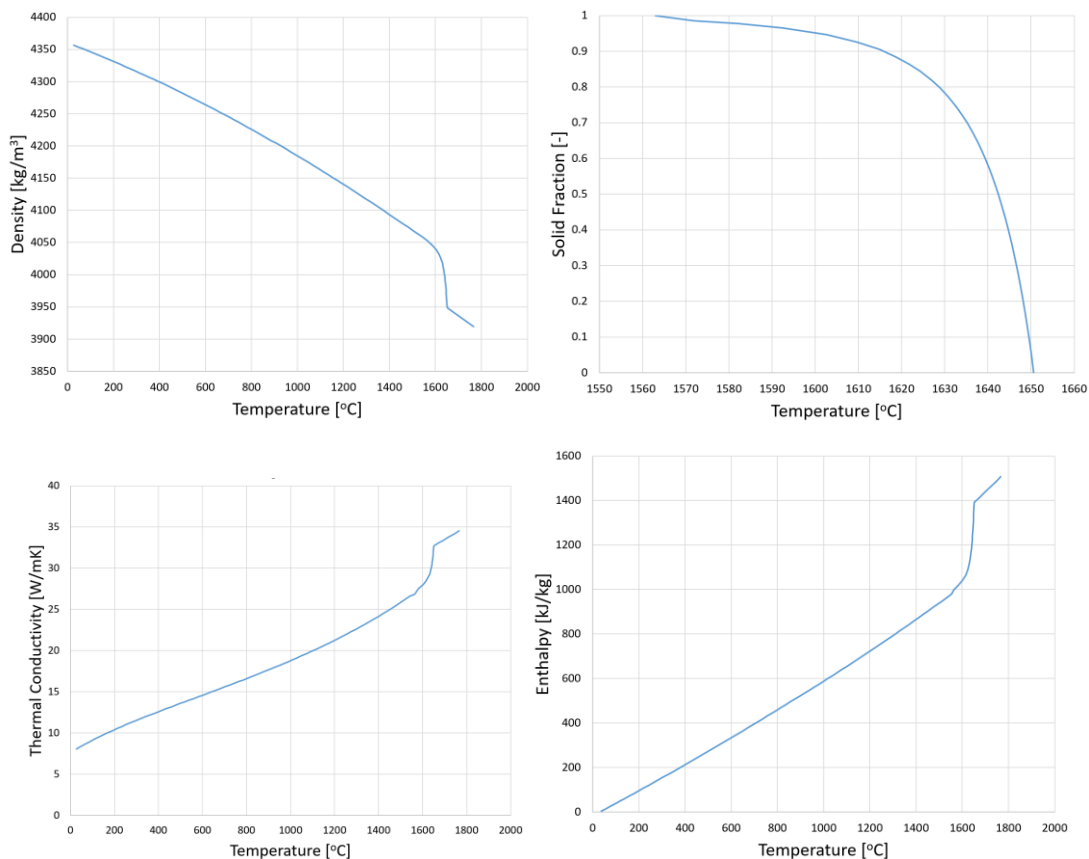
Figure 21: Preliminary design of inner (left) and outer (right) fittings.

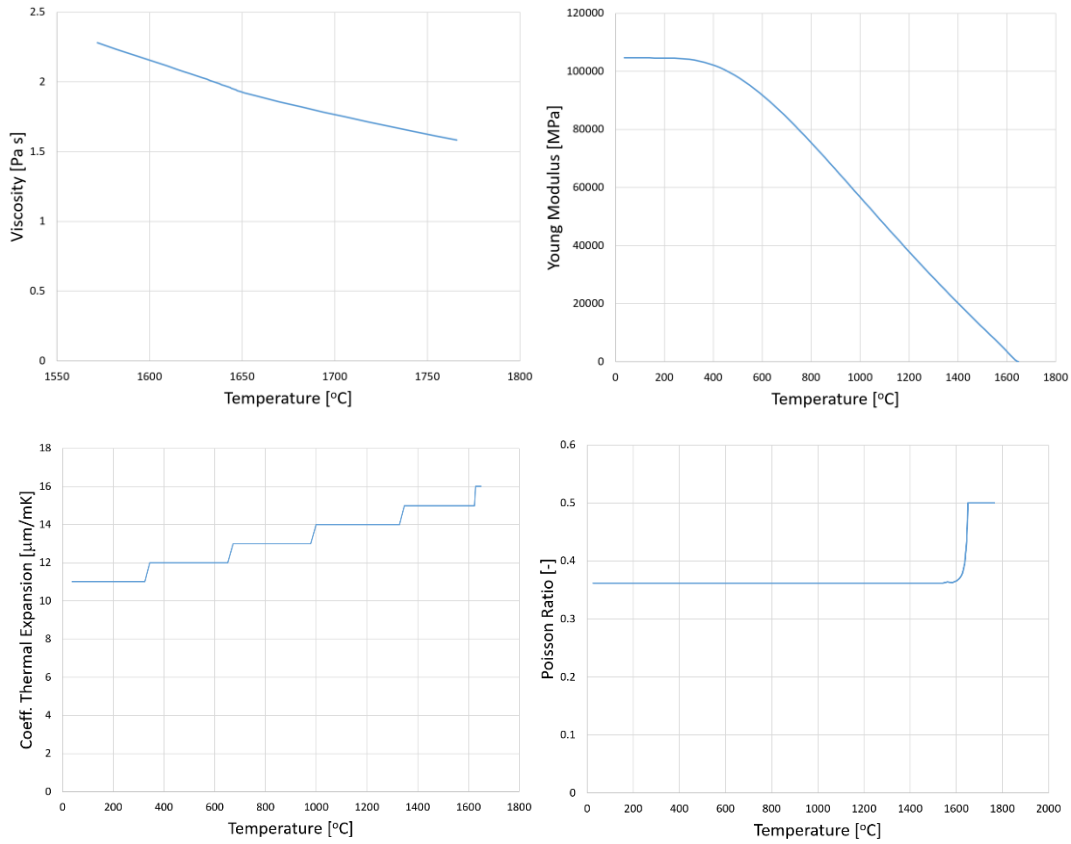
The designs correspond to those of traditional manufacturing procedures (e.g. casting). Additive manufacturing design freedom is not taken advantage of at this stage. It can be observed that one side of either design is more massive than the other one. This will impact

manufacturability and will require a dedicated effort towards identifying the optimal print orientation. Since this version of the design is preliminary, this additional effort is not pursued, and the parts' build orientation is assumed to be that of the CAD file provided by GKN.

4.1 Material

The fittings are foreseen to be manufactured using TiAl6V4, which is a material that had been often used in L-PBF for various aerospace applications. The material properties required for the different models described in D2.1 under section 3.4 are calculated using CALPHAD tools. The cooling rate in L-PBF is estimated to be approximately 106 K/s, leading to rapid solidification and limited diffusion during solidification. Scheil calculations are thus performed to obtain the solidification path and the phase evolution. The thermos-physical and mechanical properties are calculated using mixture models and the corresponding pure element properties. The results are summarized as temperature dependent plots below and are used in the different models accordingly.





4.2 Inner fitting distortion analysis

We assume that the CAD model was delivered showing the build orientation as seen in Figure 22. This orientation exhibits large overhanging areas requiring the use of suitable support structures. The critical angle for Support generation is defined to be 30°. The generated computation grid and the corresponding support structure (gray lines) are shown in Figure 23.

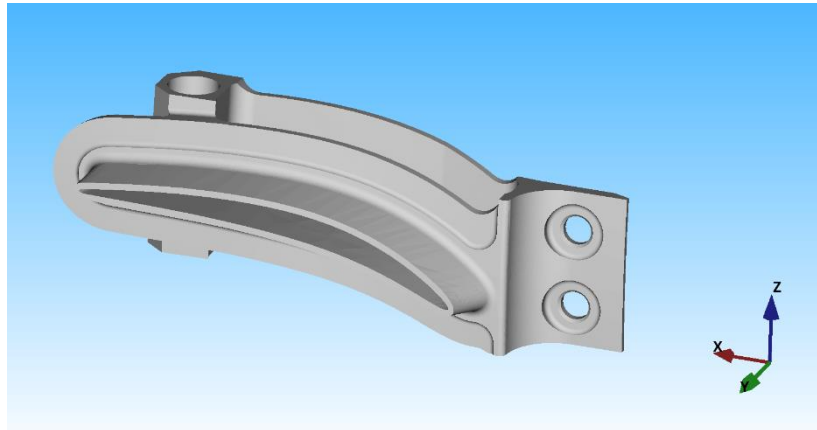


Figure 22: Build orientation of inner fitting: The Z axis shows the build direction.

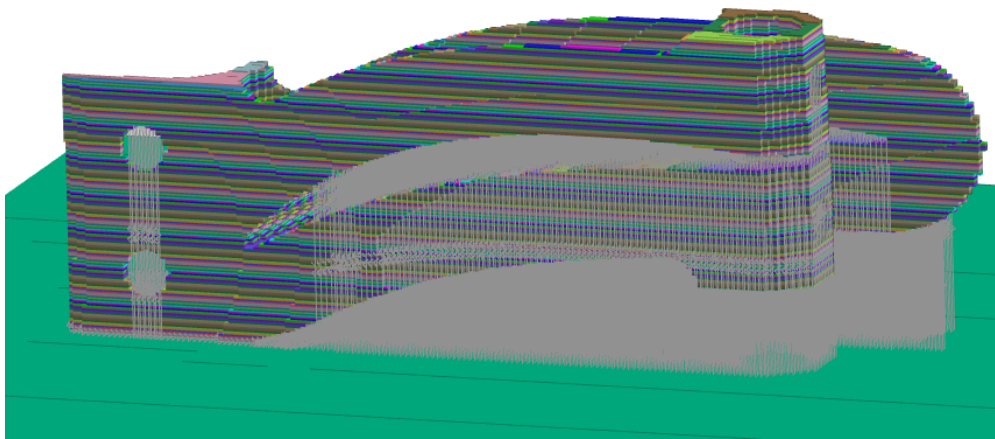


Figure 23: Inner fitting computational grid for distortion analysis and support structure generated.

Two grid resolutions are tested to ensure that grid independence is achieved. The build process, release of base plate clamps and the removal of the part from the base plate via EDM are modelled, the corresponding distortion states are shown in Figure 24.

Stress relief and heat treatment are not accounted for in these calculations, thus giving us the final as-built shape of the inner fitting.

It can be readily seen that whereas the coarse grid is computationally efficient, the distortion values are over estimated. The fine grid shows a more realistic distribution of distortion magnitudes as confirmed by further analysis of resolution effects.

The maximum distortion magnitude is predicted to be in the order of 1 mm after releasing the clamps and 4.5 mm after EDM, which are considered to be excessive distortion levels that cannot be accepted as final part shape. This behavior is attributed to the difference of mass on either side of the plate highlighted above in addition to an unfortunate orientation, where the support structure cannot efficiently counteract against distortions in the horizontal plane.

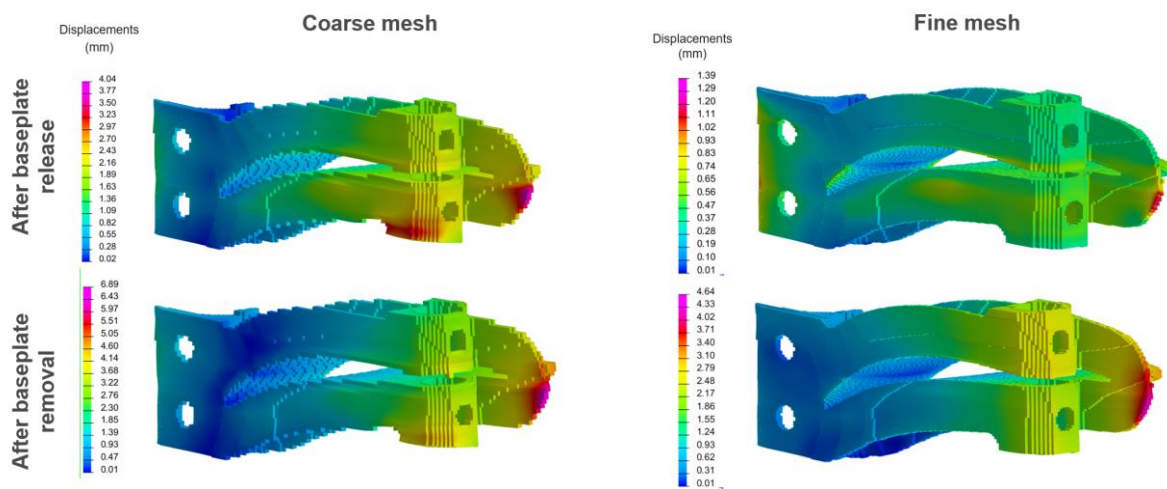


Figure 24: Distortion states after release of base plate clamps and after part removal via EDM for both a coarse grid calculation and a fine grid.

To mitigate such defects, the following options can be considered:

- Compensate for distortion by adapting the design mirroring the final distortion in the opposite direction to give as CAD conformal build,
- Oriente the part and use massive support structure to hold the part in place during building. Stress relief will have to be the first post processing step for this option.

The mitigation options are not applied here, since the design is to change and are noted accordingly to be applied on the new design, once available.

4.3 Outer fitting distortion analysis

Similar assumptions and procedure are followed for the inner fitting. The computational grid and the support structure (orange) are shown in Figure 25.

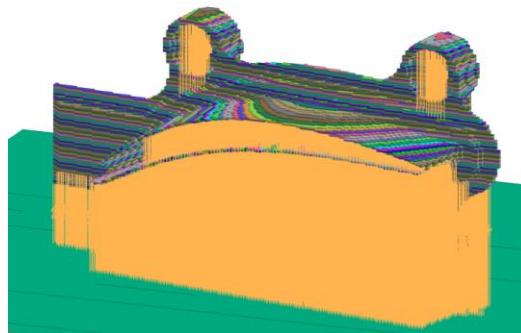


Figure 25: Distortion computational grid and support structure for inner fitting.

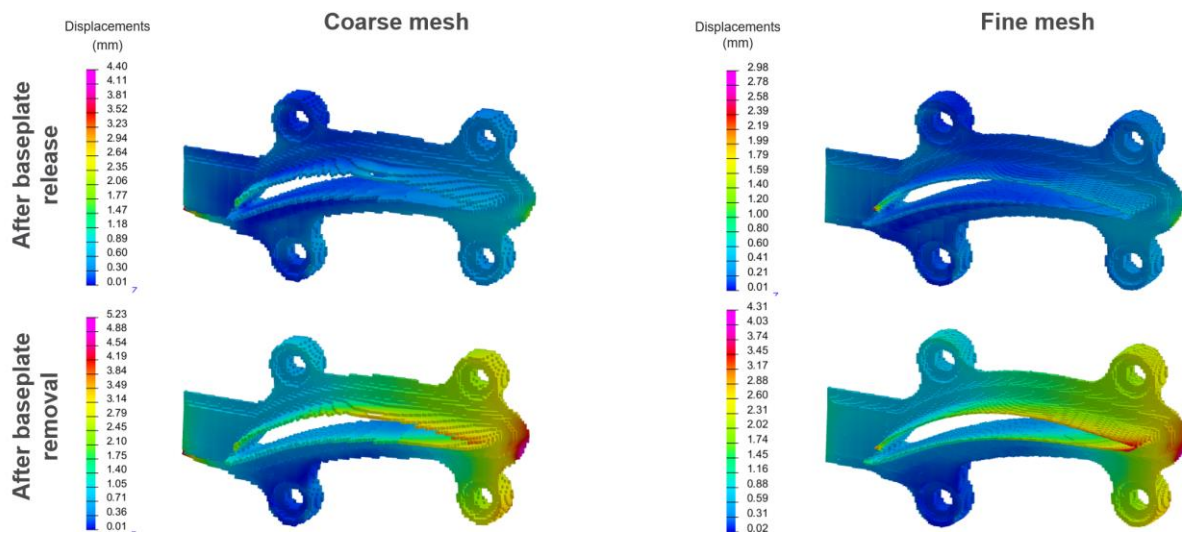


Figure 26: Inner distortion distribution.

Figure 26 shows the same trends as those found for the inner fitting. The distortion magnitudes are lower, mainly attributed to the differences in mass on either side of the central plate. Again, the misbalance of mass and the unfortunate orientation led to large distortions, which must be mitigated as suggested above.

5 RTM MODELLING & SIMULATION: RTM DIGITAL TWIN

5.1 Resin Transfer Molding (RTM) process for composite parts

The Resin Transfer Molding (RTM) process for composite parts is a closed-mold manufacturing technique used to produce high-quality, complex-shaped components from reinforced

polymer composites. Here's a general description different steps of the RTM process for composite parts:

- 1° Fiber reinforcement preforms, such as carbon fibers for aeronautical applications, placement into the mold. The layup of the preform is here realized with an Automated Fiber Placement (AFP) process (see deliverable D4.1),
- 2° Mold closure, creating a sealed cavity that defines the shape of the final part,
- 3° Resin injection: a liquid resin, the thermosetting polymer here, RTM6 for aeronautical applications, is injected into the closed mold under pressure. The resin flows through the fiber reinforcement, impregnating it completely,
- 4° Curing: the resin is allowed to cure and harden within the mold. The curing process is often accelerated by applying heat to the mold,
- 5° Demolding: the mold is opened, and the newly formed composite part is removed,
- NB: Shape distortions of the parts can occur in the curing and in the demolding phases and generate geometrical deviations on the functional surfaces of the composite parts.

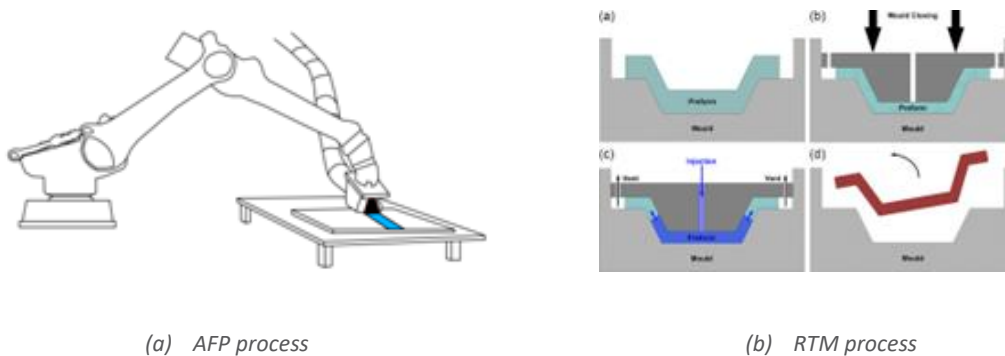


Figure 27: Draping the stacking from UD tape with Automated Fiber Placement (AFP) process & Resin Transfer Molding (RTM) process for composite parts.

5.2 RTM process modelling and simulation with PAM-RTM/DISTORTION®

RTM process models in PAM-RTM/DISTORTION®

The RTM process simulation of the composite parts is realized with a high-fidelity Multiphysics model on PAM-RTM/DISTORTION®. The RTM process combines several coupled physical phenomena: fluid mechanics represented in the resin flow, heat transfer, chemical reaction,

with the resin polymerization kinetics, in addition to solid mechanics due to the potential deformation of the composite part in the curing and the demolding.

Based on PAM-RTM[®] and PAM-DISTORTION[®] software, these models allow to consider the different steps of an RTM process:

- the filling of the composite parts, based on fluid mechanics, with incompressible, viscous flow through a porous medium and a Darcy law,
- the curing of the composite parts, based on heat balance equation in presence of curing kinetics (Kamal-Sourour model),
- the demolding of the composite parts, based on a linear thermo-viscoelasticity law for anisotropic and thermo-chemo-rheologically model of material.

Thus, the flow of the incompressible fluid is governed, if change of thickness is neglected, by the simplified form of the mass balance equation:

$$\nabla \cdot (V) = 0$$

where V is the velocity vector. Darcy's law describes the flow of Newtonian fluids through porous media. It relates the velocity vector to the permeability tensor K , the resin viscosity μ and the pressure gradient ∇P :

$$V = -\frac{K}{\mu} \nabla P$$

The energy balance equation governs the heat transfer problem. The terms of the energy balance equation on the left-hand side are respectively from left to right: the transient and advection terms. On the right-hand side of the equation, the first part of the equation is the conduction term. The term q is the volumetric heat generation related to resin polymerization.

$$\rho c_p \partial T / \partial t + \rho_r c_{p,r} V \cdot (\nabla T) = -\nabla \cdot (\lambda \cdot \nabla T) + q$$

where T is the temperature, ρ and ρ_r are the composite and the resin density. c_p and $c_{p,r}$ are the composite and the resin specific heat capacity. The subscript r denotes the resin. λ is the thermal conductivity of the composite material.

$$q = \rho_r \Delta H d\alpha / dt$$

where ΔH is the total enthalpy of reaction and α is the degree of polymerization. A kinetic law is required to calculate the polymerization rate $\partial\alpha/\partial t$ as a function of the degree of polymerization α and the temperature T . Kamal-Sourour's model is the native model in PAM-RTM®:

$$d\alpha/dt = (A_1 \exp(E_1/T) + A_2 \exp(E_2/T) \alpha^a)(B - \alpha)^b$$

where A_i are the rate constants with an Arrhenius type of dependence with temperature, E_i are the energies of activation of the chemical reaction, and a and b are exponents characterizing the sensitivity of each autocatalytic reaction. The value of B for many resin types was assumed as 1.0. In the curing phase of the RTM process, some thermal and degree of polymerization variations ΔT and $\Delta\alpha$ can occur in the part. So, resulting thermal strains ε_{ij}^T and chemical strains ε_{ij}^C can be written as:

$$\varepsilon_{ij}^T = \alpha_{ij}\Delta T$$

$$\varepsilon_{ij}^C = \beta_{ij}\Delta\alpha$$

where α_{ij} is the coefficient of thermal expansion tensor and β_{ij} is the coefficient of chemical shrinkage tensor. When the resin reaches gelation, the resin becomes rubbery. From this point the resin can sustain stress. When the resin reaches the glass transition temperature, the resin becomes glassy. In PAM-DISTORTION®, a linear thermo-viscoelasticity for anisotropic and thermo-chemo-rheologically materials behavior model is implemented, with the stress tensor σ_{ij} function of C_{ijkl} the relaxation modulus tensor, given by a generalized Maxwell model with P Maxwell elements in parallel with a free spring, ε_{ij} and $\dot{\varepsilon}_{ij}$. Thus, deformations and residual stresses can occur during the curing phase and in a second step, during the demolding.

RTM process simulation and results in PAM-RTM/DISTORTION®

The results of the RTM and demolding process are:

- the pressure and temperature fields evolution in the part and the mold during filling,
- the filling time,
- the generation of porosities and dry zones in the parts,

- the degree of cure and curing time, and the temperature evolution during curing,
- the shapes distortions in demolding.

All these process results are driven by:

- the RTM process control parameters:
 - the pressure and the temperature of the resin flow in the preform and in the mold,
 - the number and the location of the injection and void points,
 - the temperature of the mold,
 - the curing temperatures,
 - ...
- the materials properties of the resin and of the preform:
 - the viscosity of the resin,
 - The kinetic properties of the resin,
 - The fiber volume fraction of the preform,
 - the permeability of the preform, resulting from AFP process layup of the plies of the preform,
 - ...

To ensure realistic simulations of the filling phase of the RTM process, TU-DELFT team realized, on the preform carbon fibers material of the CAELESTIS project, the permeabilities characterization. The experimental process of the permeabilities measurements used and the results are available in the TU-DELFT report (REF. 5.1). The experimental permeability values of in-plane and out-of-plane K_1 , K_2 and K_3 are given, in function of fiber volume fractions in **Figure 28** and **Figure 29**. The measurements are realized on nominal stacking, without preform defects.

(REF. 5.1): Report "Caelestis permeability characterization results", 25/02/2024, TU-DELFT

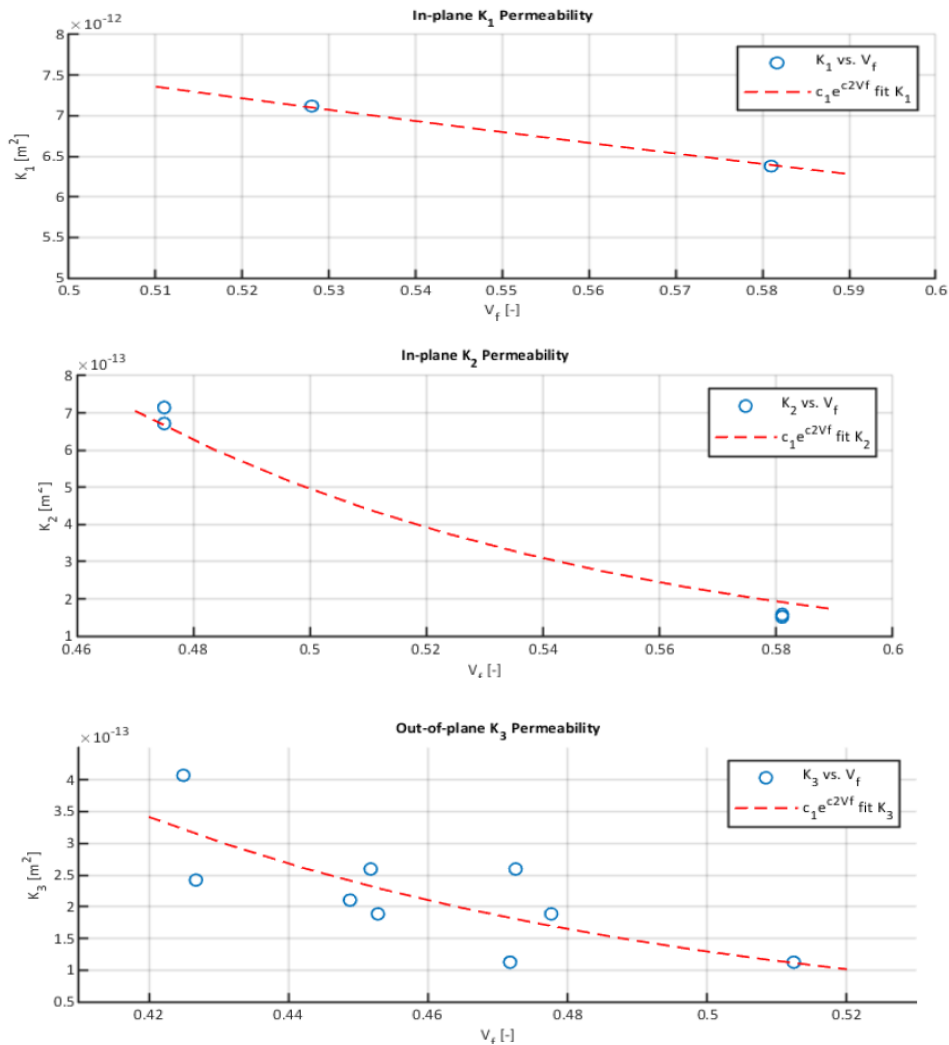


Figure 28: Permeabilities characterization and values function of fiber volume fraction (REF. 5.1).

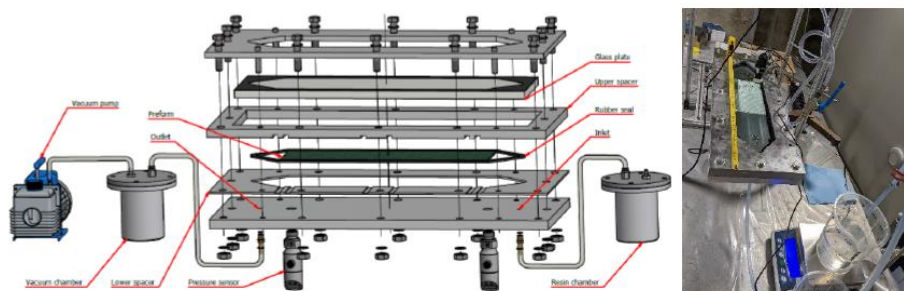


Figure 29: Flat panel setup for the in plane permeabilities characterization (REF. 5.1).

RTM process simulation in PAM-RTM/DISTORTION® with preform defects

Notice that the permeabilities values of the preform directly depend on:

- the UD fibers material, here carbon fibers,

- the stacking and the orientation of the plies,
- the presence of defects in the layup in the AFP process:
 - misalignments defects,
 - gaps defects,
 - overlaps defects.

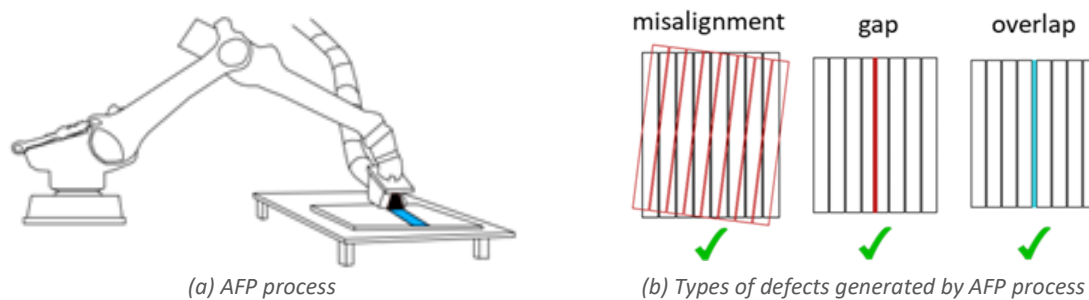


Figure 30: Draping the stacking from UD tape with AFP (Automated Fiber Placement) process & defects on plies.

Generated by AFP process, the misalignment of the plies, the gaps and overlaps between the plies in the preform can be modeled at two levels:

- 1° directly in PAM-RTM[®], with an automatic strategy developed in Python[®] and based on the native functions of the software:
 - for the misalignments of the plies, the PAM-RTM[®] native function which allows the definition of the orientation of each ply in a layup is used and customized, with a Python[®] script, to introduce some angle variations, which can be identified as the result of the AFP head orientation errors,
 - for the gaps in the plies, preferential flow paths are defined in PAM-RTM[®], with a Python[®] script, at the good locations and with the good dimensions, in the plies, which can be identified as the result of the AFP head position errors,
 - for the overlaps in the plies, local increases of the fiber volume fraction are defined in PAM-RTM[®], with a Python[®] script, at the good locations and with the good dimensions, in the plies, which can be identified as the result of the AFP head position errors.
- 2° as an input coming from ADDPath[®] software and permeability surrogate model, with the introduction of modified permeability tensors, in the numerical exchange file,

at the localization of the defects (see previous chapters in this deliverable and the deliverable 4.1). The effects of the different defects are thus considered at the level of the permeability values in the RTM simulation, estimated for each finite element of the mesh.

- NB: one of the main objectives of the CAELESTIS project is to realize a numerical workflow between software. So, the second strategy is the main one of the project (see **Figure 1** and **Figure 2**).

In the CAELESTIS project, the main results of the RTM process Digital Twin will be the shape distortions of the composite parts and the porosities fields in the composite material. The distortions are given by PAM-DISTORTION® simulations.

5.3 Proofs Of Concepts 1, 2 and OGV. Strategy for Processes Digital Twins and numerical workflow

To ensure the increasing of the complexity of the models, and to introduce step by step physical and numerical features, three models of POCs have been defined since the beginning of the WP4:

- the POC1, a plane part of UD plies,
- the POC2, a curved part of UD plies (not presented in this deliverable, see RP1-18 PERIODIC TECHNICAL REPORT (PART B)),
- the real GKN's OGV, the industrial use-case of the CAELESTIS project.

For each POC, the scientific and technological objectives were given in **Table 5**.

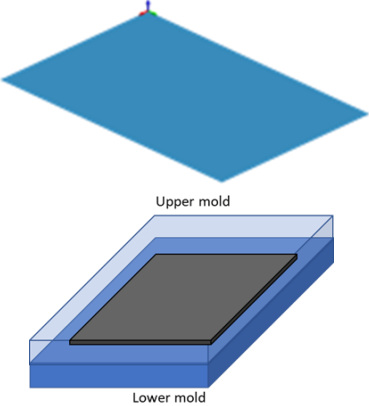
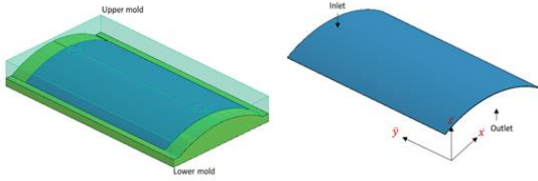
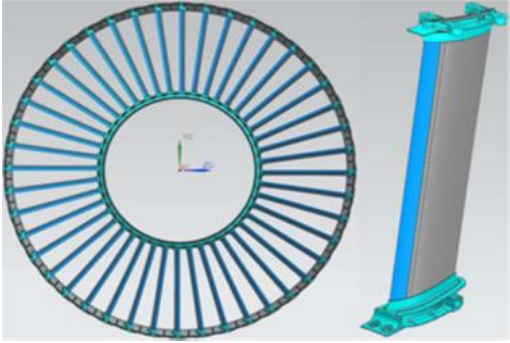
Proof of Concept	Scientific and technological objectives
 <p>(a) POC1: thin composite plate, with mold</p>	<ul style="list-style-type: none"> - 1° to identify the physical parameters which can be exchanged between the different software as input / output data - 2° to define the numerical files and format to exchange input / output data between software - 3° to model AFP and RTM process & permeability & voids at RVE level - 4° to realize a first prototype of numerical workflow between software - 5° to define and model process defects - 6° to model the plies drop-offs + insert (for AFP & RTM) - 7° DOE tool for parametric study to explore RTM process
 <p>(b) POC2: thin curved composite part, with mold</p>	<ul style="list-style-type: none"> - 1° to model a curved geometry and local orientation of plies in the composite preform - 2° to model the plies drop-offs on a complex geometry - 3° to model defects (for AFP & RTM) - 4° to optimize the numerical workflow and input / output data exchanges between software
 <p>(c) OGV composite and metallic parts, OGV assembly</p>	<ul style="list-style-type: none"> -1° to introduce real material parameters, resin thermal dependency, ...coming from physical test, commercial datasheets, and literature - 2° to consider the real process boundary conditions: metallic insert, tooling and thermal conditions - 3° to optimize the plies drop-offs for a complex geometry - 4° to model defects (for AFP & RTM) - 5° to validate the layup & filling strategies - 6° to demonstrate the readiness and the efficiency of the numerical workflow on the final POC, with all the software: OGV

Table 5: Definition of POCs and tasks for the development of digital twins and numerical physical workflow.

5.4 Proof Of Concept 1: RTM modelling and simulation

POC 1 and mold design and specification

The POC1 is the easy one. It is a composite plate of 10 carbon fibers UD plies. The length, width and height of the plate are equal to 310x160x2mm.

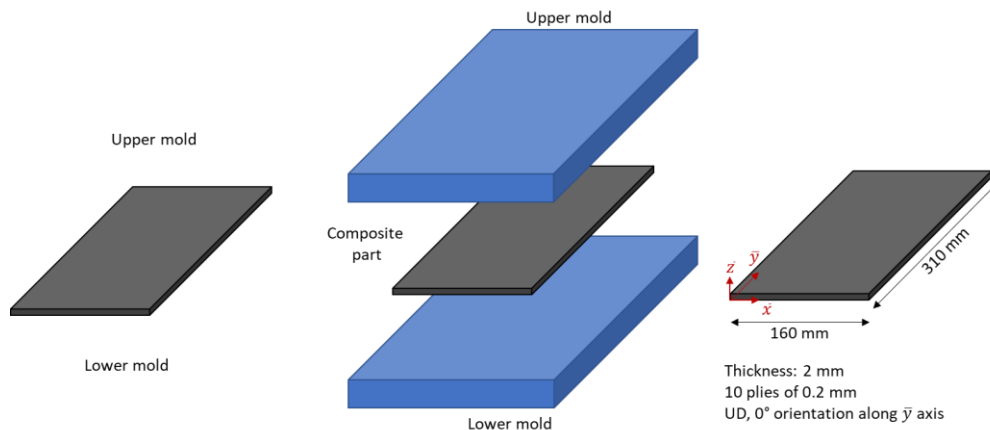


Figure 31: Dimensions and specifications of the composite plate POC1 and of the mold.

The stacking of the carbon fibers preform has 10 UD plies of 0.2mm with the orientations $[0^\circ/0^\circ/0^\circ/0^\circ/0^\circ/0^\circ/0^\circ/0^\circ/0^\circ/0^\circ]$. The resin is an Hexcel's HexFlow[®] RTM6.

Notice that the mold, the process and the design of the POC1 have been defined by AIMEN in the Work-Package 6.

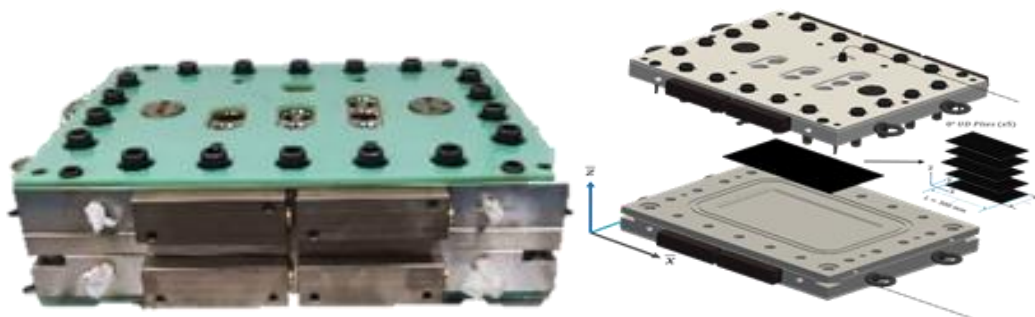


Figure 32: RTM mold for the manufacturing of the composite plate POC1.

RTM process model in PAM-RTM/DISTORTION[®]

The mesh of the POC1 in PAM-RTM/DISTORTION[®] is realized with tetrahedron finite elements. The number of finite elements is equal to 60720. The size of each finite element is around 7mm. The meshing is defined fine enough to capture with good precision the distortions of the part in the curing and in the demolding phases.

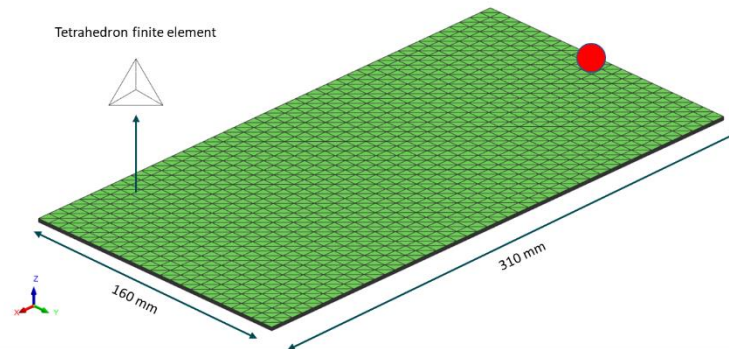


Figure 33: FEM mesh with tetrahedron 3D elements of the POC1 & injection point location.

The stacking of the preform in the mold in PAM-RTM/DISTORTION[®] is shown in Figure 34.

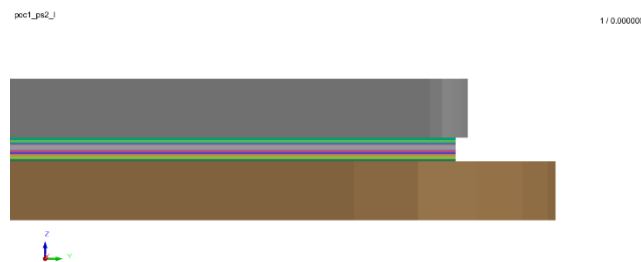


Figure 34: Stacking of the plies of the preform of the POC1.

All the material properties come from commercial datasheets for the RTM6 resin and UD carbon fibers tapes or from literature. To feed the materials cards of the different models of PAM-RTM/DISTORTION[®], a very significative number of material properties is necessary. To limit the size of chapter 5 of the deliverable D4.2, this list is not given in this report. The permeabilities of the UD carbon fibers tapes have been characterized by TU-DELFT team (REF. 5.1).

RTM process simulation and results in PAM-RTM/DISTORTION[®], without and with preform defects

The RTM process parameters used for the simulation are:

- the resin injection pressure is equal to 3 bars for the filling phase, with the location of the injection point shown in Figure 33 (red point),
- the resin injection temperature is equal to 80°C for the filling phase,

- the temperature of the mold is equal to 120°C for the filling phase,
- the temperature of the mold is equal to 180°C for the curing phase, with temperature ramp shown in Figure 35.

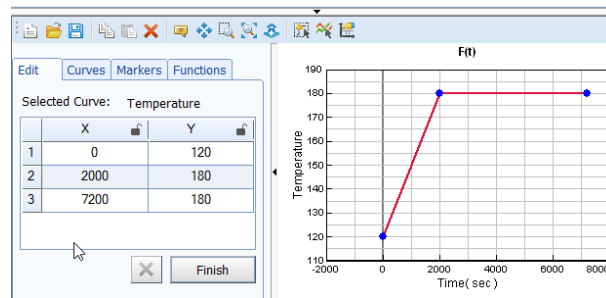


Figure 35: Temperature ramp for the curing phase of the POC 1.

The RTM process simulations on PAM-RTM /DISTORTION® offer such process results as the filling time, the pressure of the resin, and of course, the distortion of the plate, under the effects of the thermal and chemical deformations and the residual stresses in the curing and the demolding phases, as shown on the Figure 36 and Figure 37.



Figure 36: RTM process simulation of the composite plate POC 1 manufacturing.

To test the impact of the defects on the preform, here, misalignments defects, with misalignments on each of the 10 plies, are introduced with a random error of the orientation, with an normal law, defined with a mean equal to 0° and a standard-deviation equal to 2°, on the UD ply at 0°, here: [-5.7°/-0.3°/-0.2°/0.3°/-0.8°/1.0°/-3.4°/1.5°/ -0.9°/2.5°]. The effects of the misalignments of the 10 plies on the different process results can be underlined in Figure

37. Some real differences can be observed on the filling time and on the distortion values and behaviors of the part in the demolding phase:

The filling time for the filling of the POC1 and the mold is equal to:

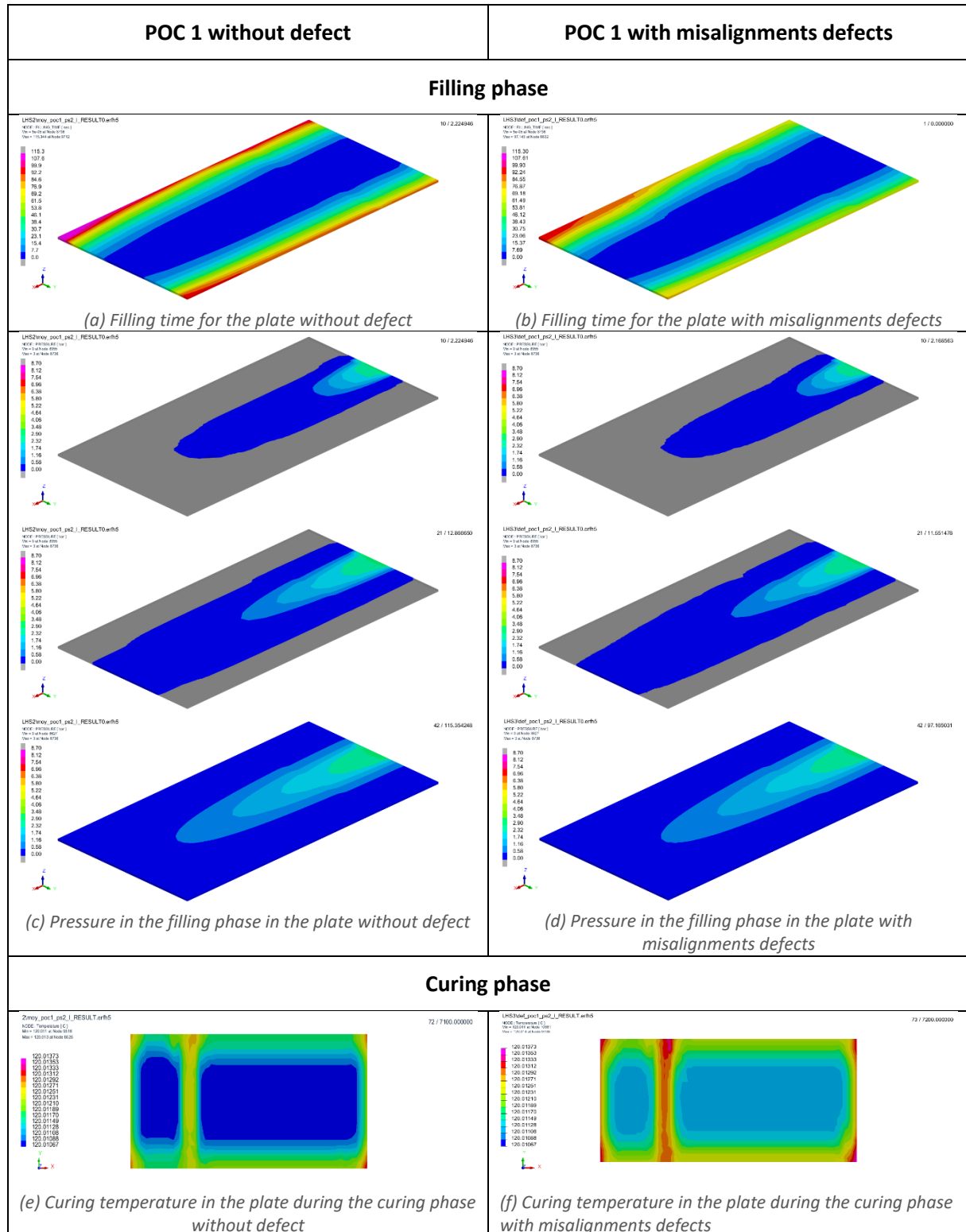
- 108 seconds for the configuration without defects of misalignment,
- 115 seconds for ta configuration with defects of misalignment,

The minimum and maximum distortions in z direction for the demolding of the POC1 are equal to:

- +/-0.01mm for the configuration without defects of misalignment,
- -0.055mm/+0.029mm for the configuration with defects of misalignment,

So, the occurrence of misalignment defects during the AFP process can have a effect on the final geometry of the part. Of course, it depends on the error of the orientation of the AFP head. However, the observed values of distortions after demolding are low and the deformation of the plate is quite similar as a “rigid body motion” of the plate, with a very low effect on the tolerances of the part.

The singularities observed on the surfaces of the POC1 during the curing phase are the results of the presence of some “holes” in the mold for the different sensors (see **Figure 37** (g) & (h)).



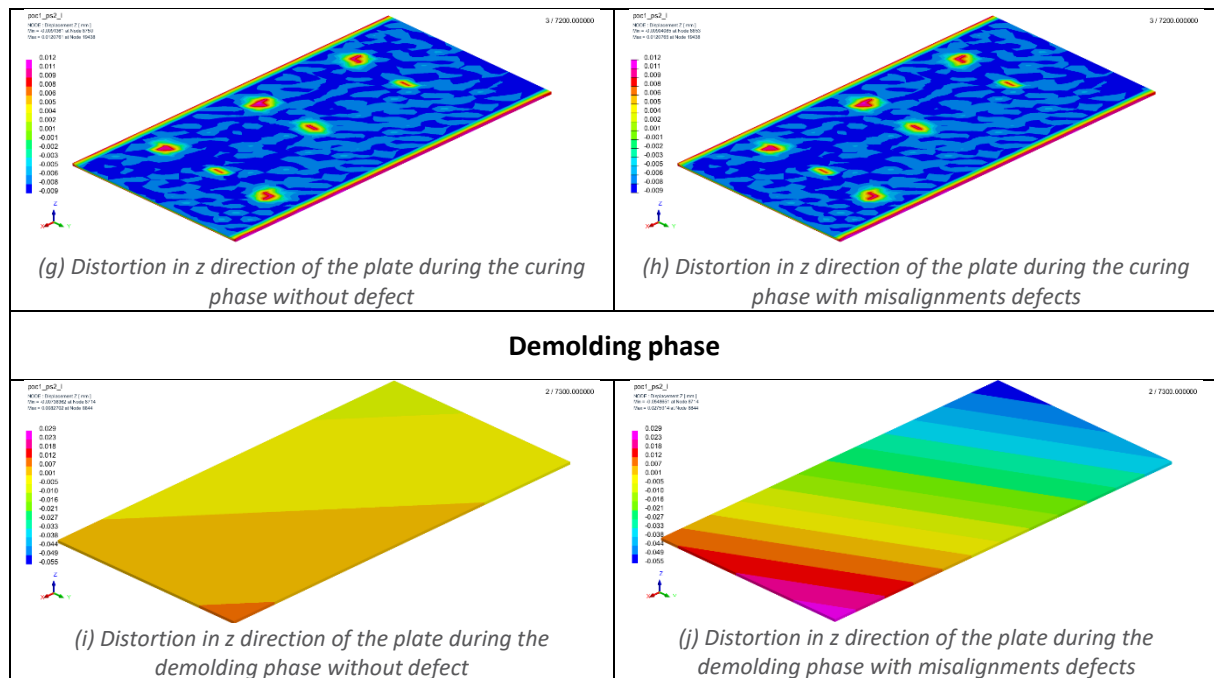


Figure 37: RTM process simulation and main results of the composite plate POC 1 manufacturing.

The total computational time of one simulation, for filling, curing and demolding, is around 15 minutes on a PC, with an Intel® Core™ i7, 2.3 GHZ, 14 cores and 20 processors, with one core used.

NB: no simulations and results are currently available for the POC1 with gaps or overlaps defects for this first version of the deliverable D.4.2.

The shape distortion of the geometry of the POC1 is a major result of the RTM process simulation for the numerical workflow of CAELESTIS project. In fact, one of the main ideas of the project is to propagate physical parameters, defects of the different processes and numerical data between each step of the global process of POC1 manufacturing:

- the AFP process simulation, with the realization of the UD preform, with the stacking of the layup, in the nominal configuration or, in a degraded configuration with defects occurrence, here misalignments, gaps and/or overlaps, transferred to the RTM process (see deliverable D4.1),
- the RTM process simulation, with the realization of the resin injection and the curing and demolding of the composite part POC1, in the nominal configuration or, in degraded configuration with defects in the preform (from AFP step) and/or RTM defects occurrence, here non-conform shape distortions, with an impact on the

tolerances on the part POC1 (see deliverable D4.3) and a non-conform porosity rate in the composite material, with an impact on the mechanical material properties (see WP3),

- the assembly process simulation of composites parts, here two plate POC1, and the tolerancing analysis of the parts, with the definition of a virtual coordinate measuring machine, and of the assembly, in nominal configuration or in non-conformed configurations with geometrical non-conformities on the tolerance's intervals on the part POC1 or on the assembly (see deliverable D4.3).

5.5 GKN's OGV: RTM modelling and simulation

5.5.1 GKN's design and specification

For this first version of the deliverable D.4.2., JVN team used the first design of the OGV, in compliance with the deliverable D1.3 "Concept of Outlet Guide Vane, preliminary design space and bill of materials", 30/11/2022, GKN report (REF. 5.2), and the CAD version of the OGV of January 2023.

The geometries and dimensions of the OGV and of the composite vane are shown on Figure 38 and Figure 39.

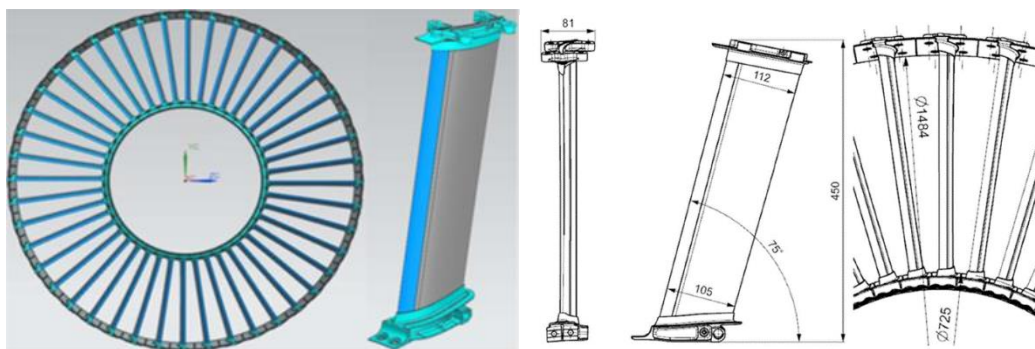


Figure 38: OGV first design and dimensions (REF. 5.2).

(REF5.2): CAELESTIS Deliverable D1.3 "Concept of Outlet Guide Vane, preliminary design space and bill of materials", 30/11/2022, GKN report

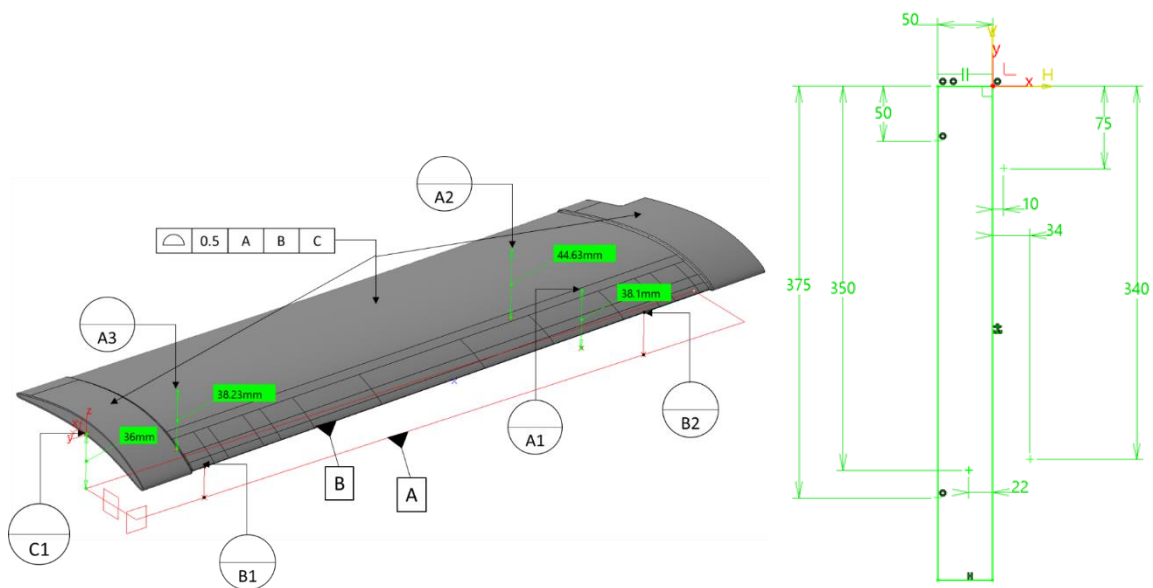


Figure 39: OGV first design and dimensions for composite vane.

“The layup of the composite vane is designed with the intent of acquiring significant tension/compression stiffness and strength in the length direction of the vane. As such zero degree plies (along the OGV span) are dominant (50%). The initial design is based on Hexcel’s 8552/AS4 carbon UD prepreg tape with CPT=0.185 mm. It is a traditional design based on a prepreg hand layup” (REF. 5.2).

However, the design of the preform has been modified to fit the AFP process and its constraints.

So, the new carbon fibers preform characteristics are:

- UD fibers carbon TeXtreme 5173,
- the tape width equal to 13 mm,
- the ply thickness equal to 0.182 mm,
- the fibers volume fraction equal to 60%,
- the number of plies equal to 40,
- the stacking and the orientations of the plies given in Figure 40.

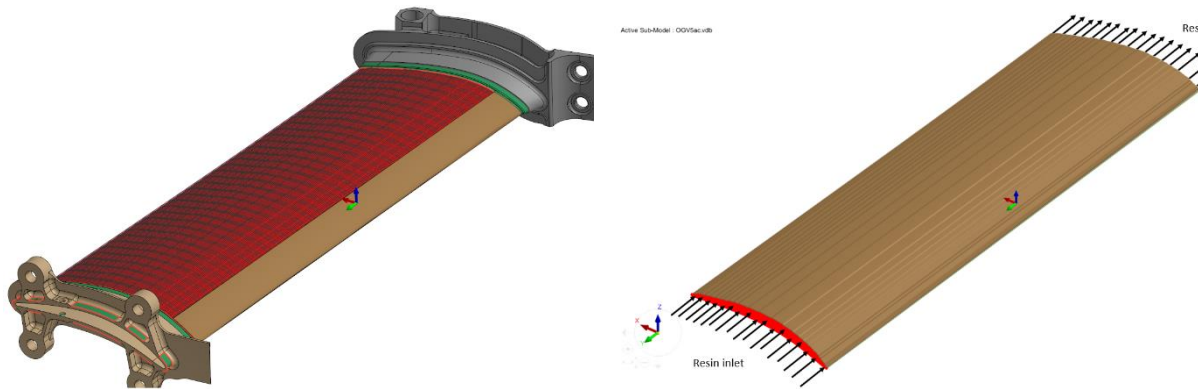


Figure 41: FEM mesh with tetrahedron 3D elements of the vane, injection strategy and "pseudo mold".

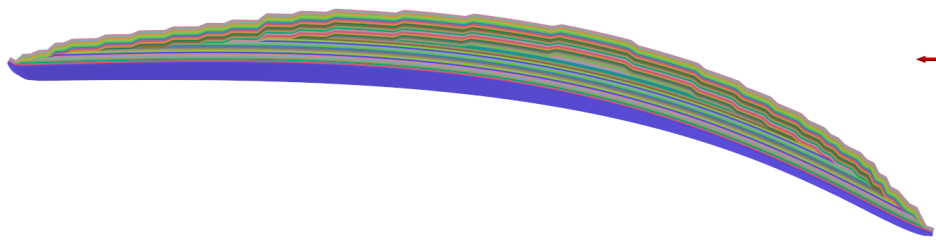


Figure 42: Stacking of the plies of the preform of the vane.

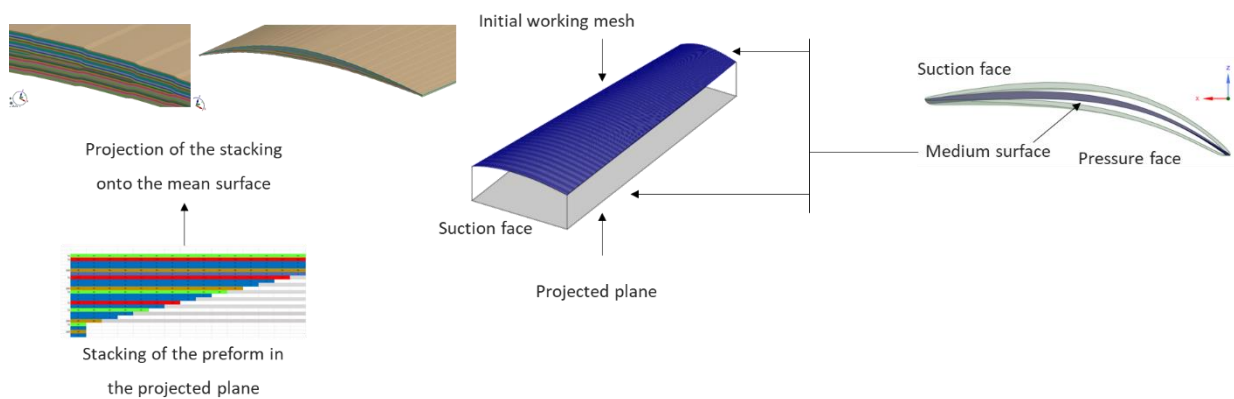


Figure 43: Automatic layup of the stacking of the 40 plies of the preform of the vane, with drop-offs management.

RTM process simulation and results in PAM-RTM/DISTORTION®

The RTM process parameters used for the simulation are:

- the resin injection pressure is equal to 2 bars for the filling phase, with the location of the injection / vent points strategy is shown in **Figure 41**,
- the resin injection temperature is equal to 80°C for the filling phase,
- the temperature of the mold is equal to 120°C for the filling phase,
- the temperature of the mold is equal to 180°C for the curing phase, with temperature ramp shown in **Figure 44**,
- NB1: the injection strategy is not currently defined by GKN at the moment of redaction of this deliverable D4.2. So JVN team did some hypotheses and proposed “a state of art” injection strategy, in compliance with the design of the vane,
- NB2: the mold of the OGV is not available at the moment of redaction of this deliverable D4.2. So JVN team did some hypotheses and proposed “a state of art” mold, in compliance with the design of the vane. So, two mold surfaces were extracted from the upper and inner aerodynamic surfaces and the inner and outer fixing parts are considered as boundary conditions of the mold in the filling and curing phases
- NB3: the inner and outer fixing parts are considered in the model in the filling and curing phases. However, at the moment of redaction of this deliverable D4.2, JVN team didn't find a solution in PAM-RTM/DISTORTION® to simulate the demolding of the vane, with the inner and the outer fixing parts, fixed at the two extremities of the vane by adhesion in the polymerization phase of the RTM process. In fact, it seems to have some interpenetrations of the geometries / the meshes of the parts, not well managed, which generate a divergence of the contact algorithm in the mechanics demolding problem. So, in this preliminary version of D4.2, the demolding results are given for the composite vane, without the effects of the two titanium parts.

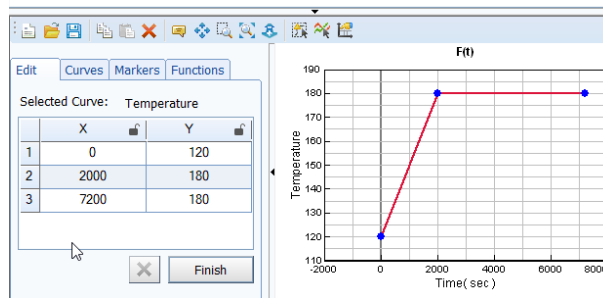
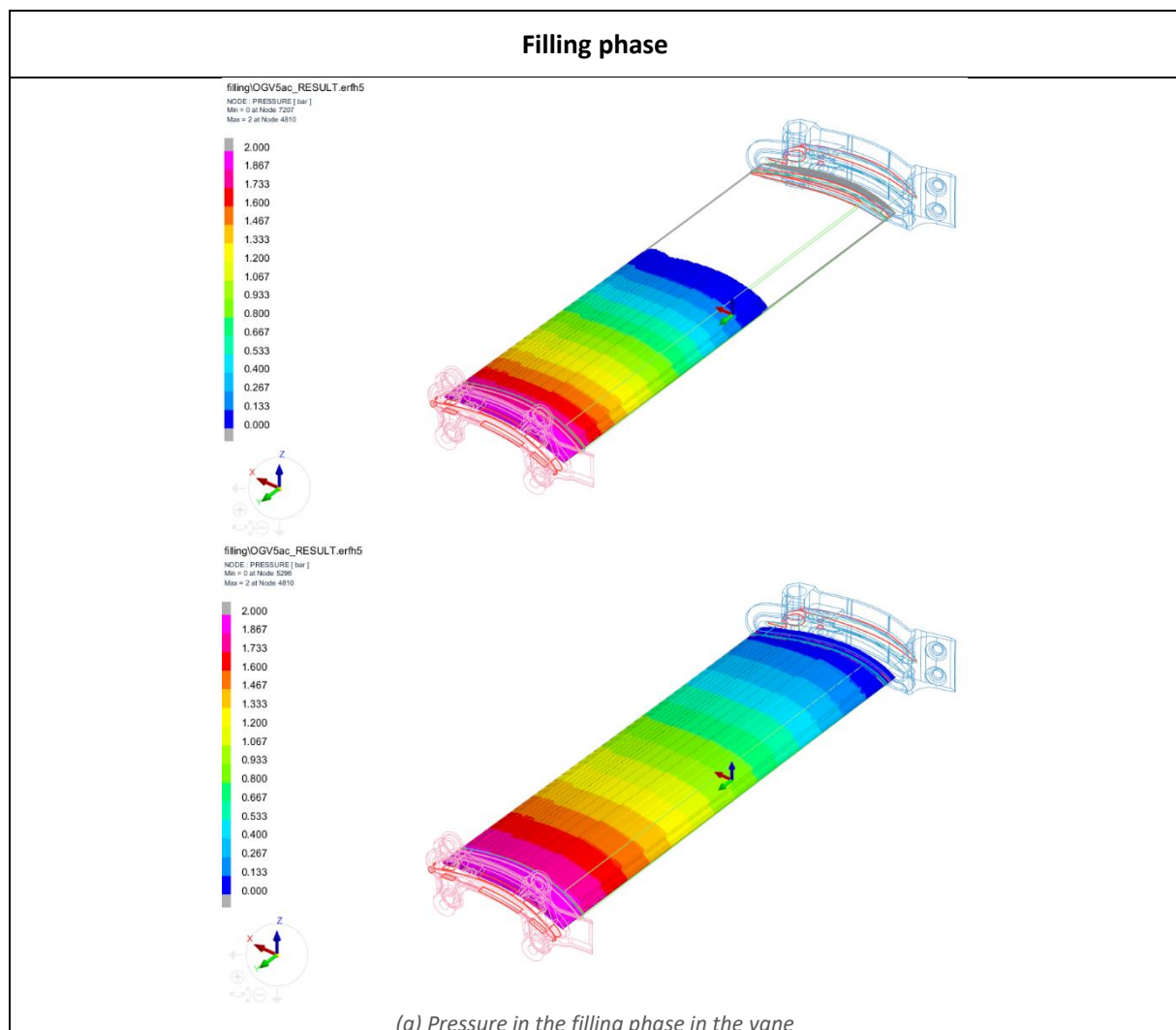


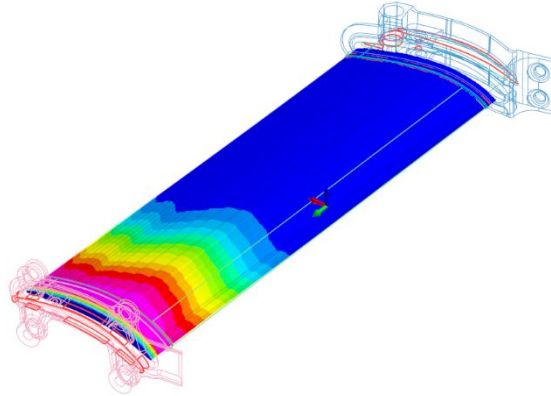
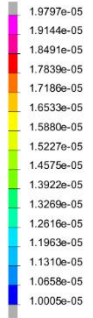
Figure 44: Temperature ramp for the curing phase of the composite vane.

The RTM process simulations on PAM-RTM /DISTORTION® offer such process results as the filling time, the pressure of the resin, and of course, the distortion of the composite vane, under the effects of the thermal and chemical deformations and the residual stresses in the curing and the demolding phases, as shown in Figure 45.

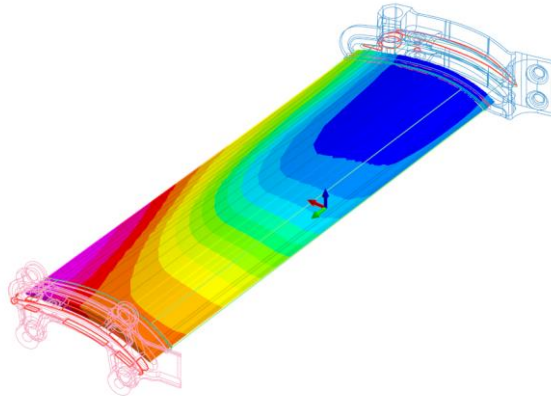
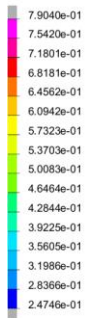


Curing phase

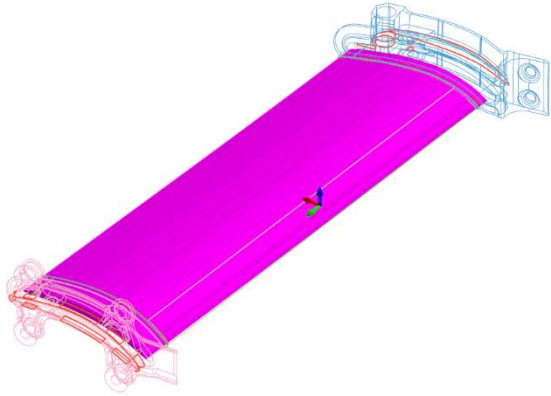
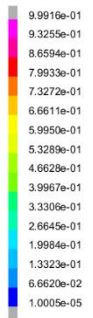
curing\OGV5ac_RESULT.ern5
 NODE : CURE
 Min = 1.0005e-05 at Node 4310
 Max = 1.9797e-05 at Node 138110



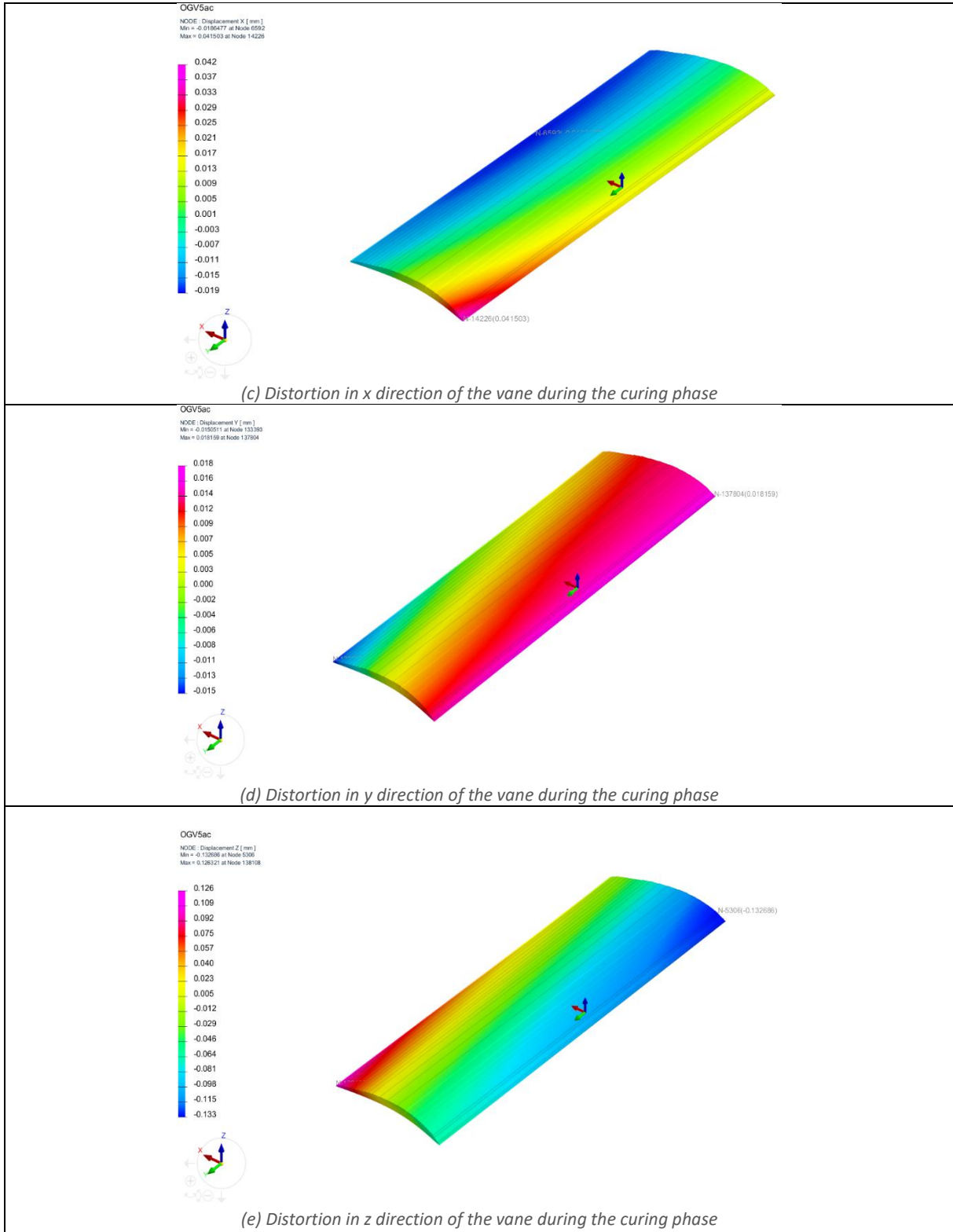
curing\OGV5ac_RESULT.ern5
 NODE : CURE
 Min = 0.247465 at Node 72987
 Max = 0.790401 at Node 14450



curing\OGV5ac_RESULT.ern5
 NODE : CURE
 Min = 0.099157 at Node 138189
 Max = 0.999157 at Node 72930



(b) Curing degree in the vane during the curing phase



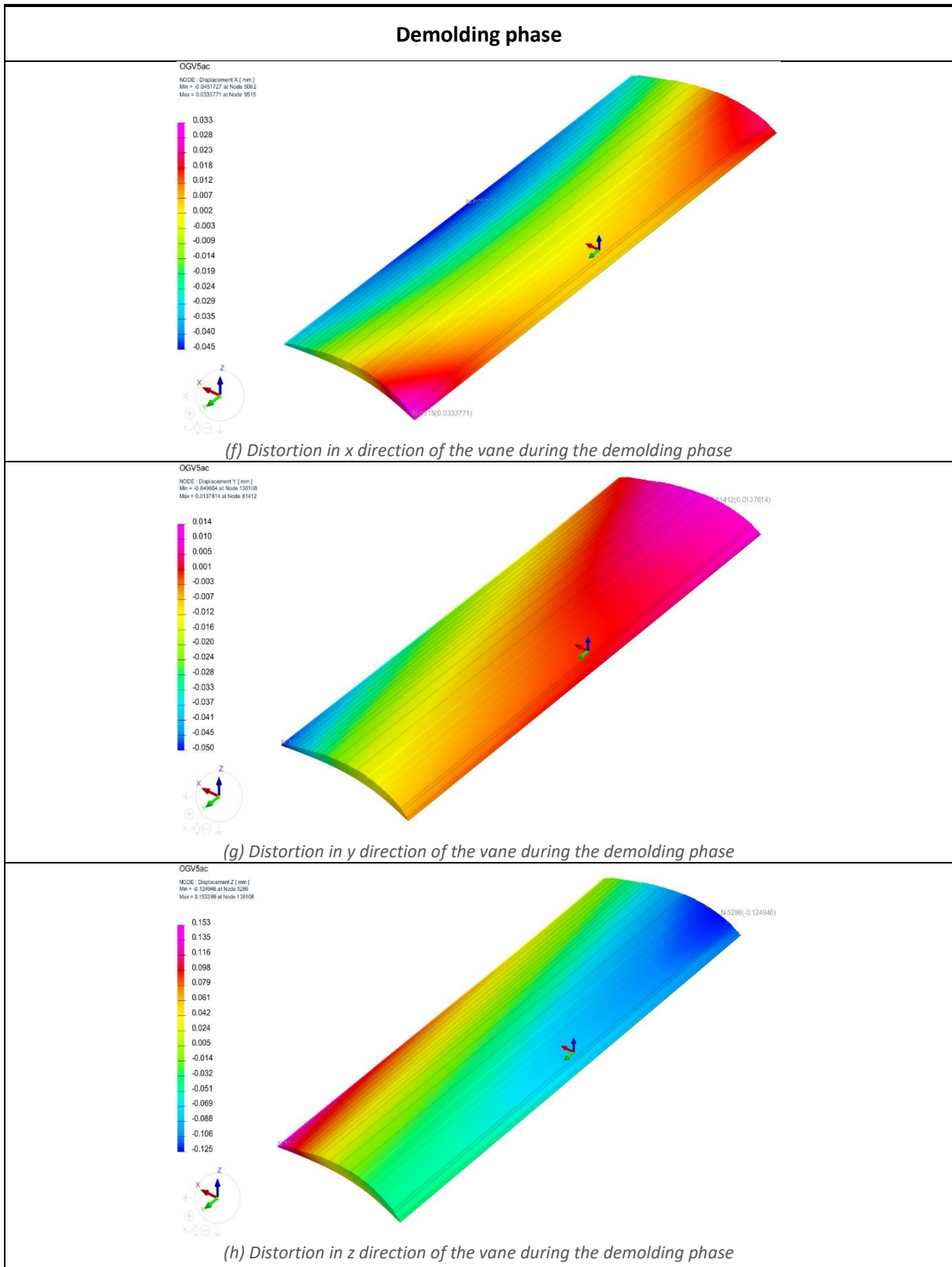


Figure 45: RTM process simulation and main results of the composite vane manufacturing.

The filling time for the filling of the vane and the mold is equal to 18 minutes for the nominal configuration of the preform and the injection strategy on the “outer fixing part” side of the vane (see Figure 41).


The minimum and maximum distortions in x, y and z directions for the curing of the vane are equal to:

- -0.019mm/+0.042mm in x direction,
- -0.015mm/+0.018mm in y direction,
- -0.133mm/+0.126mm in z direction,

The minimum and maximum distortions in x, y and z directions for the demolding of the vane are equal to:

- -0.045mm/+0.033mm in x direction,
- -0.050mm/+0.014mm in y direction,
- -0.125mm/+0.153mm in z direction,

So, the shape distortions of the surfaces of the OGV have some effect on the final geometry of the part, mainly in the z direction. Unsymmetric distortions are observed on the vane after demolding, with a global “torsion” deformation between the “outer” and “inner” side of the OGV. This asymmetry in distortion can be explained by the final geometry of the vane, imposed by the mold, by the presence of the outer and inner fixing parts in the simulations of filling and curing and by the complex stacking of the preform with plies drop-offs. Of course, it depends on the injection strategy of the vane in the RTM process. Notice that GKN specified a surface profile tolerance on the surfaces of the vane equal to 0.5, in compliance with the datums A, B and C:

	0.5	A	B	C
---	-----	---	---	---

The observed vane distortions after demolding seem to comply with the surface profile tolerance specification. In the final versions of the deliverables D4.2 and D4.3, the JVN team will try to estimate the value of this specification, with a virtual coordinate machine, using the sets of virtual coordinates measurements points at the nodes of the non-deformed mesh and of the deformed mesh (see deliverable 4.3, illustration on POC1 of the virtual CMM).

The computational times of one simulation are:

- for the filling phase, 8h15,
- for the curing phase, 8min,
- and for the demolding phase, 54 minutes,

on a PC, with an Intel® Core™ i7 2.4 GHz, 14 cores and 20 processors, with 4 cores used.

NB: no simulations and results are currently available for the OGV with misalignments, gaps or overlaps defects for this first version of the deliverable D.4.2. No numerical workflow between software is done. These tasks will be realized for the final version of deliverable D4.2, with the final design of the OGV and the real injection strategy and mold, not available now.

6 CONCLUSION AND FUTURE WORK (ITA, JVN, ESI)

In this deliverable, the operation of the digital twin for the Resin Transfer Molding (RTM) and Laser Powder Bed Fusion (L-PBF) processes, as well as its integration within the comprehensive simulation workflow of the CAELESTIS project, has been presented. Additionally, each of the simulations required for the model's implementation has been described: two-phase simulations designed to generate a model suitable for integration into PAM-RTM that predicts void formation in the RTM process based on flow conditions; L-PBF simulations capable of forecasting the final distortion of metal inserts inserted into the RTM mold; and RTM simulations where the void models and final L-PBF geometries are incorporated to simulate the mold filling process, resin curing, and final deformation of the manufactured part.

Finally, preliminary results from all the simulations presented have been showcased as an initial stage leading to final results on the Fan Outlet Guide Vane (FOGV). These results will be updated in the final version of the deliverable, expected in June 2024.

Therefore, the remaining tasks will involve leveraging the generated simulation models to conduct various simulations aimed at obtaining refined results for each of the disciplines considered in preparation for parametric studies towards the final component design.